Algorithm Theoretical Basis Document

OLCI Terrestrial Chlorophyll Index (OTCI)

MERIS Terrestrial Chlorophyll Index (MTCI) (4th Reprocessing)

Date: 30-April-2020

Issue: 2

Revision: 1

Title: OLCI Terrestrial Chlorophyll Index (OTCI)

MERIS Terrestrial Chlorophyll Index (MTCI) (4th Reprocessing)

Issue: 2

Revision: 1

Date: 30-April-2020

Signature Table

	Name	Function	Company	Signature	Date
Prepared	**Jadu Dash**	**WP Manager**	**University of Southampton**		
	Gary Watmough	**PDRA**	**University of Southampton**		
	Julio Pastor-Guzman	**Research Assistant**	**University of Southampton**		
	Luke Brown	**Research Assistant**	**University of Southampton**		
Approved					
Released					

Table of Contents

1 List of Figures

2 List of tables

3 Acronyms and Abbreviations

AATSR	Advanced Along Track Scanning Radiometer
AOT	Aerosol Optical Thickness
ATBD	Algorithm Theoretical Basis Document
ATCOR	Atmospheric and Topographic Correction for Satellite Imagery
ARSF	Airborne Research and Survey Facility
BOA	Bottom of Atmosphere
BRDF	Bi-directional reflectance function
CCC	Chlorophyll Concentration
ESA	European Space Agency
ESU	Elementary Sampling Unit
FLIGHT	Forest Light Interaction Model
FR	Full Resolution
GMES	Global Monitoring for Environment and Security
L2	Level 2
LAI	Leaf Area Index
LUT	Look-Up Table
MERIS	Medium Spectral Resolution Imaging Spectrometer
MODO	Front-end software for MODTRAN-4 radiative transfer code
MTCI	MERIS Terrestrial Chlorophyll Index
NDVI	Normalized Difference Vegetation Index
NIR	Near-infrared
NRT	Near-real Time
OLCI	Ocean and Land Instrument
OTCI	OLCI Terrestrial Chlorophyll Index
PROSAIL	Combination of PROSPECT and SAIL canopy models
RE	Red-edge
REP	Red-edge Position
RMSE	Root Mean Square Error
RP	Red Position
RR	Reduced Resolution
S-3	Sentinel-3
SAA	Solar Azimuth Angle
SAIL	Scattering by Arbitrarily Inclined Leaves
SDI	Soil Discrimination Index

SMAC	Simplified Method for the Atmospheric Correction of satellite measurements
SSD	Spatial Sampling Distance
SZA	Solar Zenith Angle
TN	Technical Note
VZA	View Zenith Angle
WP	Work Package

4 Purpose and Scope

This Algorithm Theoretical Basis Document (ATBD) describes the algorithm used to estimate chlorophyll content over land from Level-1 OLCI products from the Sentinel 3 mission. The algorithm called the OLCI Terrestrial Chlorophyll Index (OTCI) is a unique chlorophyll index for OLCI data. This document identifies the source of input data; outlines the physical principles and mathematical background; provides a justification for the algorithm selection and then explores its limitations and assumptions.

This document is split into five main scientific sections, each dealing with a different aspect of the OTCI. Section 5 provides some scientific background to the Terrestrial Chlorophyll Index (TCI) algorithm and specifically that for the OTCI algorithm. Section 6 provides the description of the mathematical algorithm including the details of the input parameters required to derive the OTCI and the output parameters. Section 6 also provides the details of the OTCI retrieval algorithm and the description of the error assessment and quality flags that have been developed. Section 7 provides details of the performance of the algorithm with particular focus on the sensitivity and limitations of the OTCI product. Section 8 gives details of the current status of the validation and Section 9 provides guidelines for future validation requirements.

4.1 MTCI 4th Reprocessing

The OTCI algorithm incorporates several improvements with respect to the MTCI released in the third MERIS reprocessing. As a result, in the fourth reprocessing, the MTCI algorithm has been updated for harmonisation with the OTCI, and this ATBD is therefore also applicable to the fourth reprocessing dataset. Where specific differences between the products exist it will clearly stated; this occurs mainly in section 7. The key changes in the fourth reprocessing are summarised below (Table 1):

Table 1: Differences between MTCI 3RP and MTCI 4RP

Change	3RP known issue	4RP evolution
Range limits	The range of MTCI values was previously restricted to between 0 and 5.5, however research suggested that this range could be increased without increasing the probability of incorporating saturated pixels.	The range limits of possible MTCI values have been updated so that MTCI values between 0 and 6.5 are now considered valid.
Uncertainties	The MTCI is subject to uncertainty due to errors in the input top-of-aerosol reflectance values, however a quantitative estimate of this uncertainty was not previously provided.	Uncertainty estimates are now provided for the MTCI, based on uncertainty propagation calculations. The standard uncertainty associated with the MTCI is determined using that associated with the top-of-aerosol reflectance values in each band.
Quality flags	The quality of the MTCI may be influenced by several non-canopy factors, however quality flags to identify pixels that could be affected by these factors were not previously provided.	A number of new quality flags are now provided for soil, viewing and illumination geometry, range and radiometry, enabling the best quality pixels to be selected by the user.

5 Scientific background of the Algorithm

5.1 Algorithm Introduction

Chlorophyll content plays an important role in determining the physiological status of a plant which is related to photosynthetic rate and varies temporarily and spatially. If we can estimate chlorophyll content in time and space, then we have a key input for models dealing with terrestrial productivity, gas exchange and vegetation health. Data derived from remote sensing can be used to estimate the chlorophyll content of leaves [RD 1; RD 2; RD 3] and canopies [RD 4, RD 5, RD 6, RD 7]. The findings in the above studies indicated that measures of reflectance in narrow red and near infrared (NIR) wavebands are required for accurate estimation. Such red and near-infrared wavebands were available as part of the MERIS sensor on board ESA Envisat mission. Dash and Curran [RD 8] developed the MERIS Terrestrial Chlorophyll Index (MTCI) to monitor vegetation conditions using an estimation of chlorophyll content derived from the reflectance values in the red-edge region of the reflectance spectra. The MTCI makes use of the vegetation spectral reflectance shift in the 'red-edge' domain. The use of the red shift means that the MTCI product remains responsive to high chlorophyll content levels where traditional vegetation indices saturate [AD1, AD2]. For instance, a recent study [RD 9] demonstrated a significant doubling of the signal to noise ratio for MTCI compared to the commonly used Normalised Difference Vegetation Index (NDVI) over areas of wooded land cover.

The MTCI algorithm has provided an operational measure of canopy chlorophyll content to users [RD 8]. The Sentinel-3 spacecraft will carry a set of optical and microwave instruments, one of which is the Ocean and Land Colour Instrument (OLCI). The OLCI will have a similar band configuration to MERIS and therefore, provides a unique opportunity to ensure the continuity of the global MTCI at the MERIS scale.

5.2 Introduction to the OLCI sensor

The Global Monitoring for Environment and Security (GMES) Sentinel-3 (S-3) mission will primarily provide data for GMES services related to the marine environment such as ocean-current forecasting. However, the mission will also provide data for land services including fire

detection and land cover mapping. To achieve this, the pair of satellites that make up Sentinel-3 will include a radar altimeter, an infrared radiometer and a wide-swath ocean and land colour radiometer. The Ocean and Land Colour Instrument (OLCI) aims to provide data continuity with the MERIS sensor on board Envisat. The S-3 satellite is scheduled for launch in 2013. With a spatial resolution of 300 m and 21 bands compared to 15 on MERIS the OLCI will be tilted 12 degrees across track to minimise the impact of sun-glint and cloud cover on the images. Having two satellites will enable a revisit time of less than two days for the OLCI at the equator and provide global coverage every 1 to 3 days. The spectral characteristics and the spatial sampling distance are shown in Table 2. More information about the mission, services and the technical details of the sensor can be found in the GMES mission requirement document [AD 3] or in the indicated web-pages [RD 10].

Table 2: Spectral characteristics and Spatial Sampling Distance (SSD) for Sentinel-3

Band	Centre λ (nm)	Spectral Width Δλ (nm)
1	400	15
2	412.5	10
3	442.5	10
4	490	10
5	510	10
6	560	10
7	620	10
8	665	10
9	673.75	7.5
10	681.25	7.5
11	708.75	10
12	753.75	7.5
13	761.25	3.75
14	764.375	3.75
15	767.5	2.5
16	778.75	15
17	865	20
18	885	10
19	900	10
20	940	20
21	1020	40

5.3 Physical/Mathematical Background to the algorithm

The spectral reflectance of vegetation is characterized by absorption features that are the result of electron transitions and vibrational stretching of organic and inorganic bonds. The main chemical constituents of leaves include; chlorophyll, water, nitrogen and carbon containing compounds which are comprised primarily of protein, lignin and cellulose. Of these constituent components, chlorophyll is associated with the process of photosynthesis and together with water, temperature, nutrient availability, CO_2 and sunlight determines the rate of primary productivity. Therefore, chlorophyll is an important driver for the whole ecosystem [RD 11]. When incoming radiation interacts with vegetation, some of the radiation is reflected, some absorbed and the rest is transmitted. A typical reflectance spectrum of a vegetation canopy can be subdivided into 3 parts; (i) visible in the region of 400 - 700 nm; (ii) near-infrared (NIR) in the region of 701 – 1300 nm, and; (iii) middle-infrared in the region of 1301 - 2500 nm.

Chlorophyll is the major absorber of radiation in the visible region. Chlorophyll are of two types; (i) chlorophyll-a, and; (ii) chlorophyll-b. Chlorophyll-a content is usually two to three times that of chlorophyll-b and dominates the absorption of incoming radiation with a wavelength between 600 - 700 nm [RD 12]. Other leaf pigments also have an important effect on the visible spectrum. For example, the yellow to orange-red pigment, carotene, has a strong absorption in the 350 - 500 nm range and is responsible for the colour of some flowers and fruits as well as leaves without chlorophyll. The red and blue pigment, xanthophyll, has strong absorption in the 350 - 500 nm range and is responsible for leaf colour in autumn.

In the near-infrared (NIR) spectral domain (701 - 1300 nm), the leaf structure can explain the optical properties. The NIR spectral region can be divided into two major spectral sub-regions: (i) between 701 and 1100 nm, where reflectance is high, except in two minor water-related absorption bands (960 and 1100 nm), and; (ii) between 1100 and 1300 nm, which corresponds to the transition between high NIR reflectance and water-related absorption bands of the middle infrared. The intensity of NIR reflectance is commonly greater in organic materials compared to reflectance from most inorganic materials. This feature gives vegetation a bright appearance in NIR wavelengths which can enable organic and inorganic materials to be deciphered relatively easily.

The middle-infrared region contains information about the absorption of radiation by water, cellulose and lignin. The protein molecules are made up of carbon, hydrogen and oxygen and nitrogen atoms. Thus, nitrogen status can be inferred indirectly by studying the absorption feature in that region [RD 13]. Other biochemicals, which contribute to absorption in middle infra-red wavelengths, are starches, sugars, lipids and minerals. Curran [RD 14] presented a list of forty-four absorption features in the visible and near-infrared wavelengths which were related to foliar biochemical constituents. The relations between multispectral reflectance and vegetation amount to six wavebands [RD 15] summarised in Table 3.

Table 3: Characteristic spectral features of foliar biochemicals (adapted from Curran, 1980).

Waveband	Waveband width (nm)	Characteristics	Relation to vegetation amount
Ultraviolet/blue	350-500	Strong chlorophyll and carotene absorption	Strong negative
Green	500-600	Reduced level of pigment absorption	Weak positive
Red	600-700	Strong chlorophyll absorption	Strong negative
Red edge	700-740	Transition between strong absorption and strong reflectance	Weak negative
Near-infrared	740-1300	High vegetation reflectance	Strong positive
Middle-infrared	1300-2500	Water, cellulose and lignin absorption	Not specific

The red-edge (RE) is a region within the transition zone between the red and NIR domains of a vegetation reflectance spectrum. The RE marks the boundary between absorption due to chlorophyll in the red region and scattering due to leaf internal structure in the NIR region [RD 16]. The red-edge position (REP) can be defined as the maximum of the first derivative of the reflectance spectra of a leaf [RD 16, RD 17]. The most commonly used techniques to estimate the REP include; (i) higher order curve fitting techniques [RD 18]; (ii) an inverted Gaussian technique [RD 19, RD 20]; (iii) a linear interpolation technique [RD 21, RD 22], and; (iv) a Lagrangian interpolation technique [RD 23]. However, REP estimation techniques have some drawbacks including saturation at high chlorophyll contents and difficulties in applying spectrally discontinuous data. Therefore, estimating the REP could not be applied to operational global

products. However, the MERIS Terrestrial Chlorophyll Index (MTCI) was developed as a surrogate estimator of the REP and applied successfully to MERIS data.

5.4 Justification for the selection of the algorithm

The MTCI is simple to calculate and yet it is sensitive to a wide range of chlorophyll content values. Furthermore, the following strengths of the MERIS sensor led to the adoption of the MTCI as an operational ESA Level 2 land product:

- The fine spectral resolution of the MERIS sensor;
- Moderate spatial resolution (300 m full resolution (FR) and 1 km reduced resolution (RR));
- Three-day revisit time, and;
- Radiometrically, it was the most accurate imaging spectrometer in space [RD 4]

MTCI is available as a standard L2 product from MERIS data as the Bottom of Atmosphere (BOA) Vegetation data product. Consequently, MERIS MTCI has shown potential for use in several applications ranging from mapping the effect of salt stress in coastal vegetation to estimate gross primary productivity for different biomes (MTCI applications are presented in Section 10).

The OTCI is designed to provide a continuation of the MTCI product. It will be sensitive to a wide range of chlorophyll content values and the range of values will be extended to provide more information about the chlorophyll content. The OTCI will have similar strengths to the MTCI as the sensors are similar in terms of radiometric, spectral and spatial resolutions. Further strengths of the OLCI sensor for the monitoring of chlorophyll content are:

- The red band (band 4) will be negatively related to chlorophyll content of vegetation;
- The red-edge band (band 5) will have a neutral relationship with the chlorophyll content of vegetation;
- The NIR band will have a positive relationship with the chlorophyll content of vegetation.

6 Mathematical algorithm description

This section provides the mathematical description of the OTCI. For continuity and added explanation the section begins with a brief description of the MTCI.

6.1 Description of the MERIS Terrestrial Chlorophyll Index (MTCI)

The MTCI is calculated as the ratio of the difference in reflectance between band 10 and band 9 and the difference in reflectance between band 9 and band 8 of the MERIS standard band setting. Equation 1 shows the band numbers used in the MTCI equation and the corresponding centre wavelengths of these bands:

$$\mathrm{MTCI} = \frac{R_{\mathrm{Band\ 10}} - R_{\mathrm{Band\ 9}}}{R_{\mathrm{Band\ 9}} - R_{\mathrm{Band\ 8}}} = \frac{R_{753.75} - R_{708.75}}{R_{708.75} - R_{681.25}} \qquad \text{Equation 1}$$

Where $R_{753.75}$, $R_{708.75}$, $R_{681.25}$ are reflectance in the centre wavelengths (nm) of the MERIS standard band setting. The MTCI product effectively combines information on Leaf Area Index (LAI) and the chlorophyll concentration (CCC) of leaves to produce an indication of chlorophyll content.

6.2 Description of the OLCI Terrestrial Chlorophyll Index (OTCI)

To ensure continuity with the MTCI the OTCI equation uses OLCI bands that are equivalent to those on MERIS. Thus, the OTCI is calculated as the ratio of the difference in reflectance between band 12 and band 11 and the difference in reflectance between band 11 and band 10 of the OLCI standard band setting. These bands have an identical band wavelength centre and spectral width to those on the MERIS sensor. Equation 6.2 describes the OTCI:

$$\mathrm{OTCI} = \frac{R_{\mathrm{Band\ 12}} - R_{\mathrm{Band\ 11}}}{R_{\mathrm{Band\ 11}} - R_{\mathrm{Band\ 10}}} = \frac{R_{753.75} - R_{708.75}}{R_{708.75} - R_{681.25}} \qquad \text{Equation 2}$$

Where R_{band12},R_{band11}, R_{band10} are the reflectance in band centred at 753, 709 and 681 nm of the OLCI sensor. Therefore, the OLCI Terrestrial Chlorophyll Index (OTCI) will be similar to MTCI the main differences will be related to the 12˚ tilt angle of the OLCI sensor.

The position of the OLCI bands are displayed in Figure 1 and overlaid is an illustrative spectral reflectance spectrum for vegetation. The low levels of reflectance in the wavelength range between 650 and 700 nm is due to the higher levels of absorption caused by chlorophyll which is captured by OLCI band 10. Reflectance levels increase sharply between OLCI band 10 and band 12.

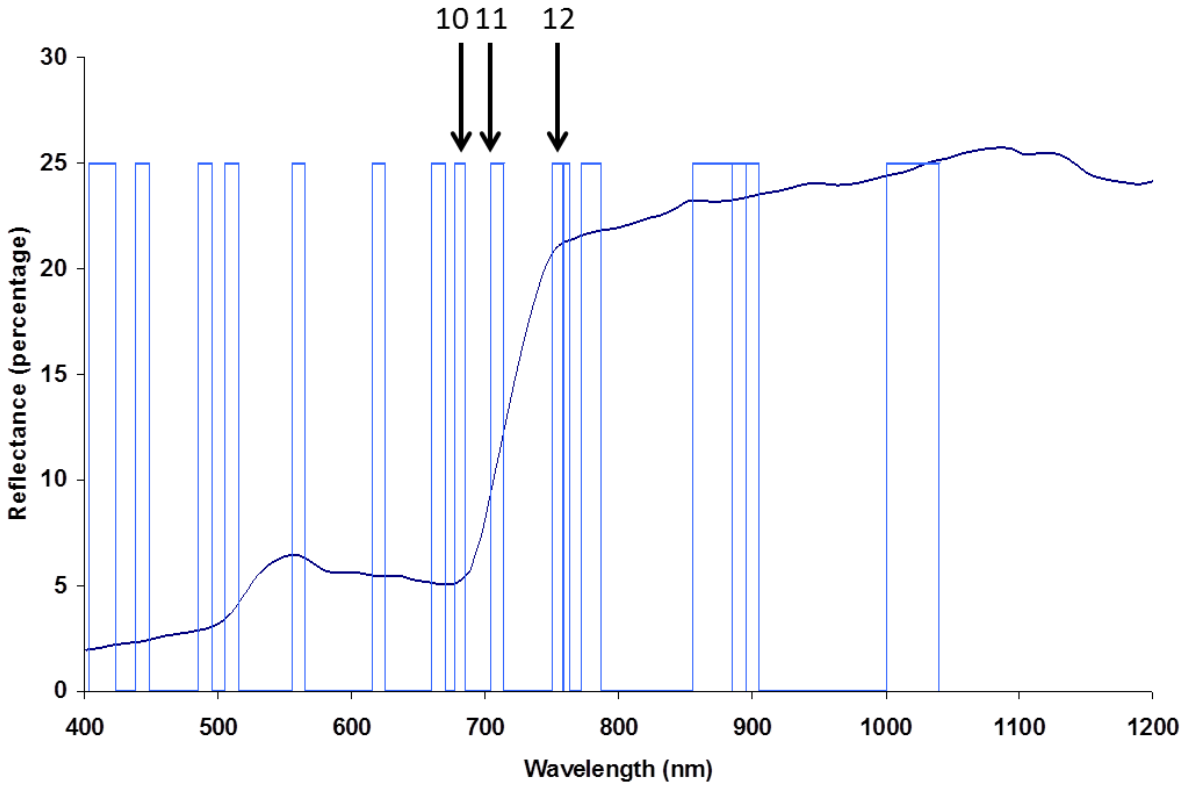

Figure 1: OLCI bands overlaid on vegetation spectra in the visible and NIR region.

6.3 Input Operational Parameters

The OTCI is classified as a Land Surface Level 2 Product in the S-3 product definition. The information in Table 4 should be used in the OLCI PRODUCT DEFINITION document.

Table 4: OTCI Product parameters

Product Name	OLCI Terrestrial Chlorophyll Index
Parameter ID	OTCI
Product Level	2
Description	Estimates the chlorophyll content in terrestrial vegetation. Aims to monitor vegetation condition and health.
Product parameters	
Coverage	Global
Packaging	Half-orbit
Latency	NRT, NTC, RP
Units	Dimensionless
Range	1-6.5
Sampling	Spatial: 260m x 290m (FR) and 1.4km x 1.16km (RR). Spectral: N/A
Format	1-byte integer
Appended Data	Error estimate (1-byte integer)
Frequency	1 product per orbit
Size of product	Approximately 0.54 GB (FR), 35 MB (RR)
Additional Information	
Input Bands	Normalised surface reflectance in Band 5, 8, 10, 11 and 12
Ancillary and Auxiliary Data	Illumination and viewing geometry. If available AOT and ortho-rectified.

The input parameters required to calculate the OTCI are detailed in Table 5 and the information in Table 5 should be used in the OLCI PRODUCT DEFINITION document.

Table 5: OTCI Input parameters

Input		
variable	Description	Range
ρ_{green}	Top of Aerosol Reflectance in green band (normally OLCI band 5 (510nm) (used for soil flag)	0-1
ρ_{red1}	Top of Aerosol Reflectance in red band (normally OLCI band 8 (665nm) (used for soil flag)	0-1
ρ_{red2}	Top of Aerosol Reflectance in red band (normally OLCI band 10 (681.75nm) (used for data quality check and OLCI calculation)	0-1
$\rho_{rededge}$	Top of Aerosol Reflectance in green band (normally OLCI band 11 (708.75nm) (used for data quality check and OLCI calculation)	0-1
ρ_{NIR1}	Top of Aerosol Reflectance in green band (normally OLCI band 12 (753.75nm) (used for data quality check and OLCI calculation)	0-1

A series of auxiliary data is also required for the OTCI algorithm and these are detailed in Table 6.

Table 6: Auxiliary data required for OTCI algorithm

Auxiliary data		
variable	Description	Range
θs	Sun zenith angle	0-70°
θv	View zenith angle	0-55°
τ_a	Aerosol optical thickness, currently there was no Aerosol data available for OTCI processing, but information from Synergy product could be used in future	
Cloud	Cloudy pixel flag	
Invalid	Invalid pixel flag	
Land	Land pixel flag	

6.4 Output Operational Parameters

The output generated from the OTCI algorithm will be an index assigned as a real number. It was found that the value for OTCI could reach over 10 in some cases. Based on experience with MTCI and results of the MTCI-EVAL project a minimum and maximum range of OTCI has been set at 0 and 6.5 respectively which can then be scaled into digital number values (1 to 255). Separate flags will be created that demonstrate if the pixel met quality criteria set out in section 6.8 of this document. Table 7 summarises the output parameters from the OTCI algorithm process.

The uncertainty variable that will be provided along with the OTCI will be calculated based on the law of propagation of uncertainty as described by Miura et al. (2000). Each of the individual data flags (Acquisition Noise, Soil, and Illumination Angle) will be added together to provide a single estimate of uncertainty for each OTCI pixel value.

Table 7: OTCI Output parameters

Output			
Variable	Description	Range	Data Type
OTCI	OLCI Terrestrial Chlorophyll Index	0 – 6.5	Floating Point
Flag 1	Soil Flag* based on Soil Discrimination Index	0/1	Unsigned integer
Flag 2	Aerosol Flag	0/1	Unsigned integer
Flag 3	Illumination/Geometry Angle Flag	0/1	Unsigned integer
Bad Data	From Level 1 processing and spectral check	0/1	Unsigned integer
Quality Flag*	This will be an 8 bit flag relating to different flags		Unsigned integer
Uncertainty	Error propagation linked to Flag 1, Flag 2 and Flag 3	% of OTCI	Floating Point

* *See Section 7.1 for a description of the soil flags*

6.5 Algorithm Flow Chart

An outline of the algorithm flow is presented in Figure 2. In order to avoid meaningless values and numerical problems, input spectra shall be screened first for clouds, water and non-vegetated land surfaces. It then includes some simple spectral tests; one of which uses an additional reflectance at a second NIR band. Based on error propagation during the processing, the expected accuracy of the product will be estimated. OTCI was originally designed for top of canopy reflectance, but its adaptation to Rayleigh corrected data in the MERIS processing chain has proven to be fairly robust to aerosol content. The baseline is thus to take Rayleigh corrected reflectance as an input. The green band (ρ_{green}) is also included in the algorithm flow chart as it is used in the soil discrimination index (SDI) which forms the soil quality flag.

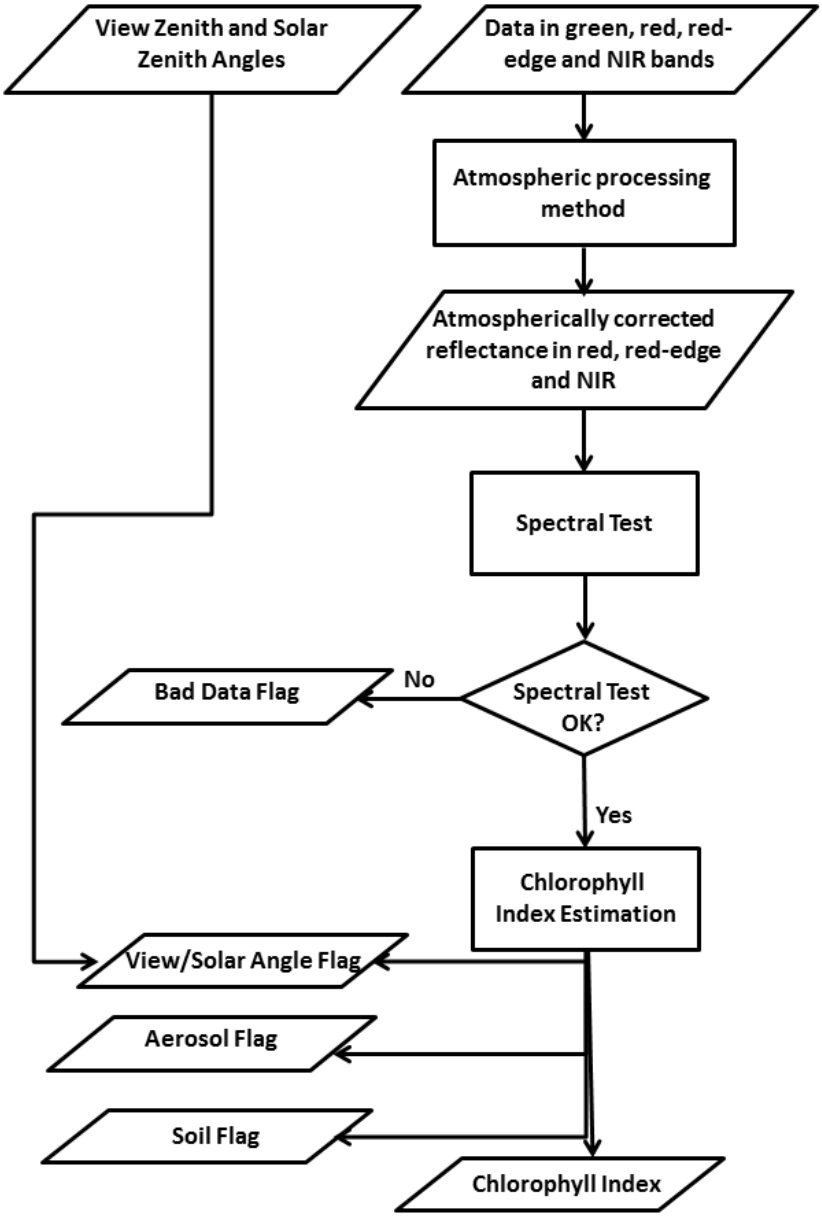

Figure 2: Outline of the chlorophyll index algorithm for OTCI.

6.6 Algorithm performance, sensitivity studies and limitations

This section provides an outline of the MTCI algorithm performance, sensitivity of the MTCI algorithm to changes in atmospheric conditions, data processing, soil background, view angle and random noise. The section finishes by assessing the overall accuracy of the MTCI algorithm taking into consideration its sensitivity to the above parameters and concludes with details of the assumptions that were made during the analysis.

6.6.1 *Performance*

The performance of the MTCI algorithm was assessed for several full orbit data sets. MTCI algorithms were run on the standard Level 2 data and a SMAC correction was applied to Level 1 data and an MTCI derived. The MTCI algorithms processing time was recorded and the number of pixels considered and the range of MTCI values estimated were also recorded.

Three full orbit datasets from the MERCI website were downloaded to explore the performance of the MTCI algorithm. The MTCI algorithm was calculated using Bands 8, 9 and 10 of the MERIS data and compared to the time it took to calculate the same MTCI algorithm using data output from the SMAC processor in BEAM. Figure 3, Figure 4 and Figure 5 show the location of the two orbits selected for this analysis.

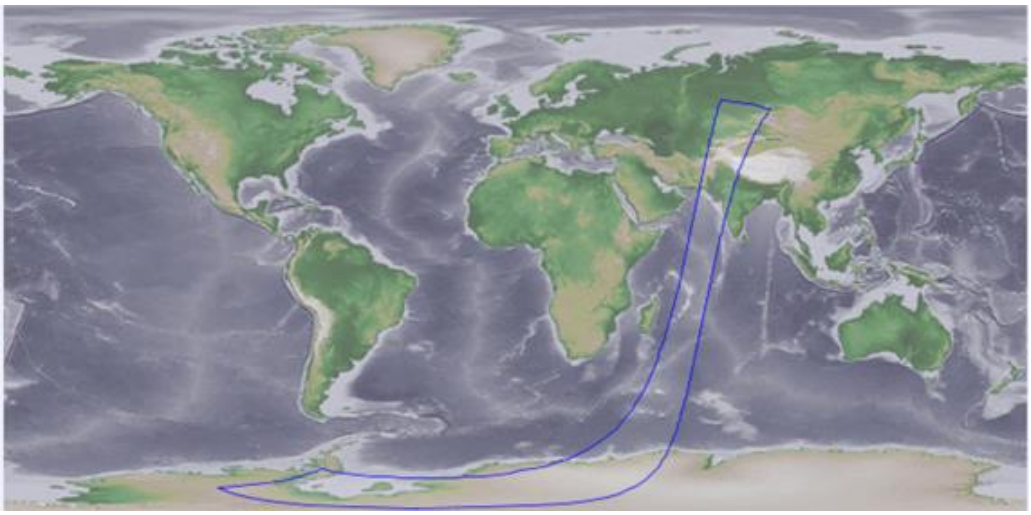

Figure 3: Location of Full orbit 1 for performance analysis

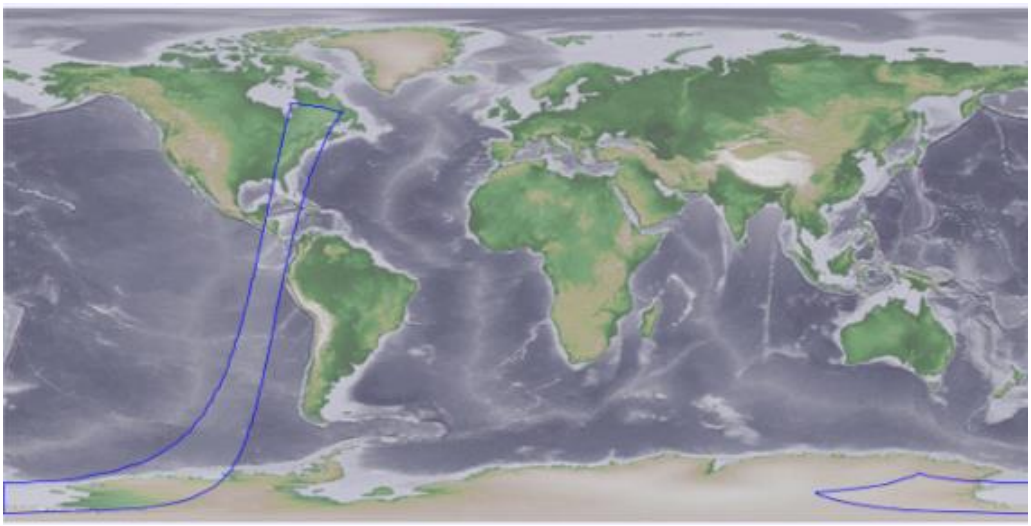

Figure 4: Location of full orbit 2 for performance analysis

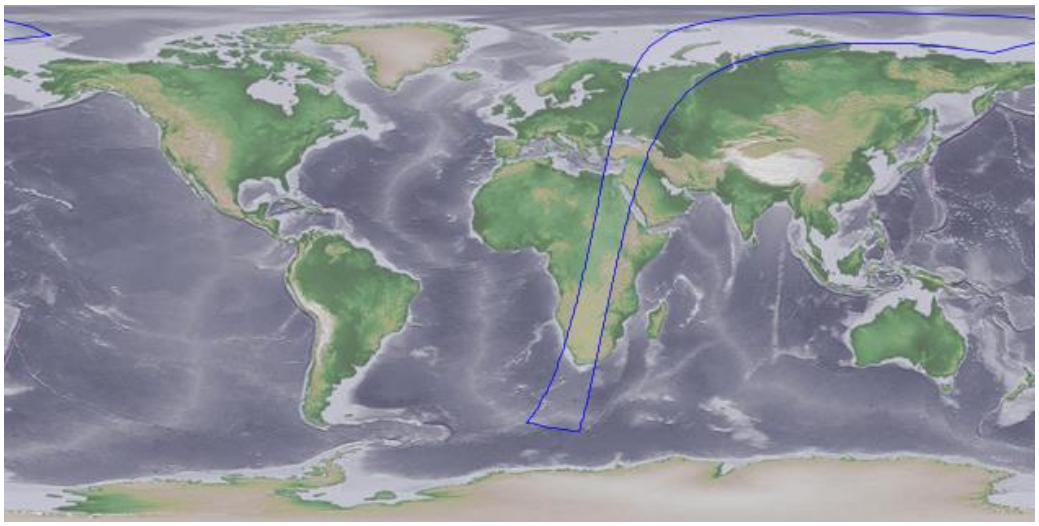

Figure 5: Location of full orbit 3 for performance analysis

The performance of the MTCI algorithm was compared to the SMAC processor and is presented in Table 8; this was based on a desktop PC with an Intel Core i5-2400 CPU @ 3.1 Ghz and 4.00 gb memory with a 64-bit operating system.

Overall, the SMAC algorithm has a small effect the MTCI values compared to the L2. SMAC does not handle cloud edges and no cloud flag is used in the SMAC processing chain. This means that cloud pixels can still be passed through the data selection stages and MTCI values estimated for areas affected by significant levels of cloud. The L2 algorithm currently in operational use for MERIS data has a cloud flag in the processing stream. It could be explored if the L2 cloud flag could be linked to the SMAC analysis and automate these to create a more stringent atmospheric correction procedure prior to the creation of L2 products. The L2 cloud mask could be used to mask out cloud prior to the SMAC atmospheric correction being run on clear pixels. This would not however account for semi-transparent cloud that was not detected by the sensor and sub-pixel problems. Overall, the differences between the L2 and SMAC MTCI values suggest that this would have a small impact on overall estimations of MTCI.

Table 8: Summary of performance statistics for MTCI calculations and SMAC processing of entire orbit datasets

	Orbit 1 L2 MTCI	Orbit 1 SMAC MTCI	Orbit 2 L2 MTCI	Orbit 2 SMAC MTCI	Orbit 3 L2 MTCI	Orbit 3 SMAC MTCI
Min	0	0	0	0	0.0005	0.006
Max	5.5	4.85	5.5	5.5	5.5	5.5
Mean	1.66	1.11	2.1	2.1	1.79	1.84
SD	0.37	0.57	0.53	0.84	0.55	0.80
Total Pixels	16681601	16681601	16681601	16681601	16087153	16087153
MTCI pixels	728132 (4.36%)	888068 (5.3%)	542250 (3.25%)	442327 (2.65%)	5195083 (30.9%)	4914726 (29.2%)
SMAC time		5 mins		5 mins		8 mins
MTCI Time	20 seconds	30 seconds	10 seconds	20 seconds	10 seconds	20 seconds
Writing SMAC file		4 mins		3 mins		3 mins

6.6.2 *Sensitivity*

A detailed assessment of OTCI sensitivity was carried out within this project. The sensitivity was defined as the difference between the observed OTCI values and the predicted OTCI values from the Earth Observation data. Five different parameters that OTCI was thought to be sensitive to were explored; (i) effect of atmospheric conditions; (ii) effect of data processing model; (iii) effect of soil background; (iv) effect of view angle, and; (v) effect of random noise.

6.6.2.1 Effect of Atmosphere

Examining the impact of atmospheric conditions is vital to ensure data products from different sensors and different time periods provide accurate estimates of MTCI. The PROSAIL model [RD25] was used to generate spectral reflectance values for a range of LAI values (LAI = 0.6, 1, 2, 3, 4, 5, 6, 7) and a Chlorophyll concentration of 40. The MODO software is a graphical front-end to the MODTRAN-4 Radiative transfer code [RD 26] and can be used to simulate spectral reflectance data for different atmospheric conditions. For each LAI value four parameters that can significantly affect the TOA reflectance values were varied one at a time:

- Aerosol optical thickness was varied 0.1, 0.3, 0.5, 0.7 and 1;
- Water Vapour was varied 0, 1.0, 2.0, 3.0, 4.0 and 5.0 g/cm^2;
- Ozone was varied 0, 0.1, 0.2, 0.3, 0.4, 0.5, 0.7, 0.9 cm-atm, and;

A baseline at sensor reflectance series was created with water vapour content of 0.01, ozone of 0.001, AOT of 0 (150 km visibility) and elevation of 0 km above sea level. This was assumed to represent a scenario where data had been atmospherically corrected and was assumed to represent top of canopy reflectance. To simulate the at-sensor reflectance due to changes in atmospheric parameters, one parameter was changed at once and the other two remained as the baseline values. So for example, during the simulations of Water vapour:

1. Water vapour = 1.0 g; Ozone = 0.001, AOT = 100km visibility;
2. Water vapour = 2.0 g; Ozone = 0.001, AOT = 100km visibility;
3. Water vapour = 3.0 g; Ozone = 0.001, AOT = 100km visibility;
4. Water vapour = 4.0 g; Ozone = 0.001, AOT = 100km visibility;
5. Water vapour = 5.0 g; Ozone = 0.001, AOT = 100km visibility.

The MODO software can be used to simulate reflectance for a range of different satellite sensors. Results here were simulated for MERIS and the resulting simulated at-sensor reflectances' were analysed to demonstrate how the reflectances fluctuated with different levels of a given atmospheric condition added.

The simulated reflectance values for MERIS bands 8, 9 and 10 were used to estimate the MTCI value and the uncertainty relating to ozone content, water vapour content and AOT were explored. The effect of varying each of the above atmospheric parameters was visualised by calculating the MTCI value and each value plotted. The effect of AOT is displayed in Figure 6, water vapour in Figure 7, ozone in Figure 8.

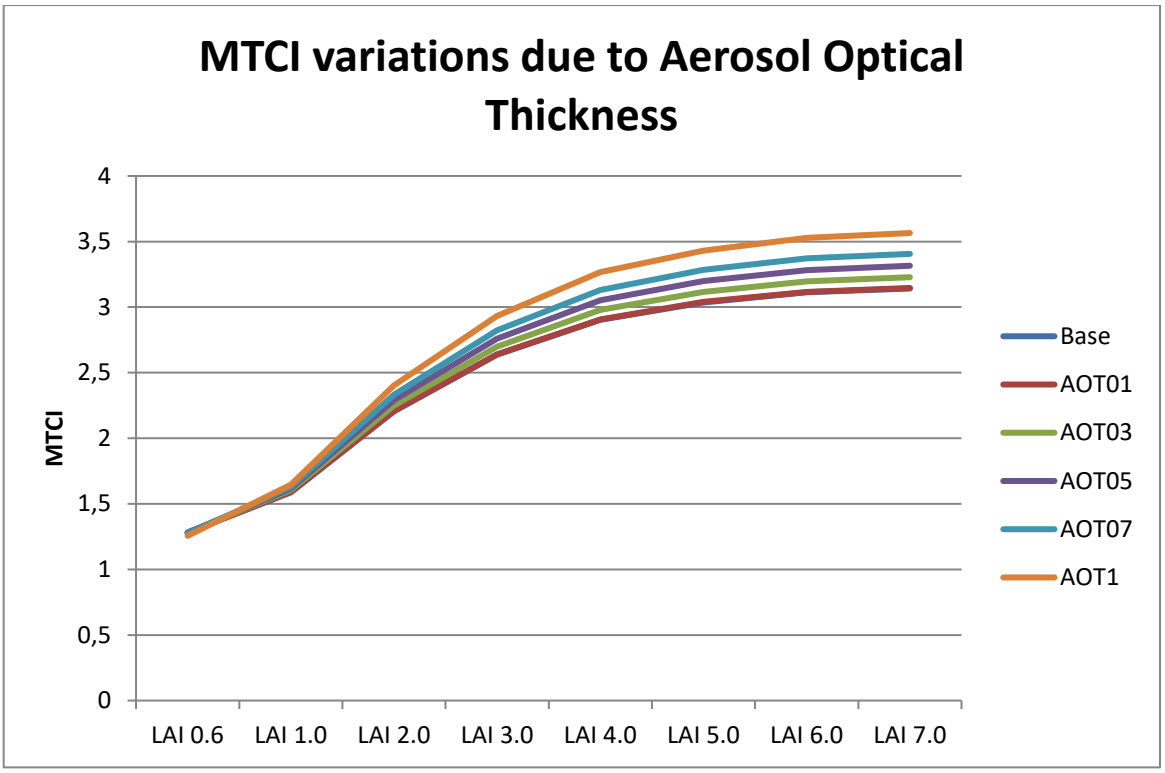

Figure 6: Reflectance fluctuations due to AOT variations. Baseline has AOT=0; Water Vapour 0.01; Ozone 0.001 and Elevation 0.

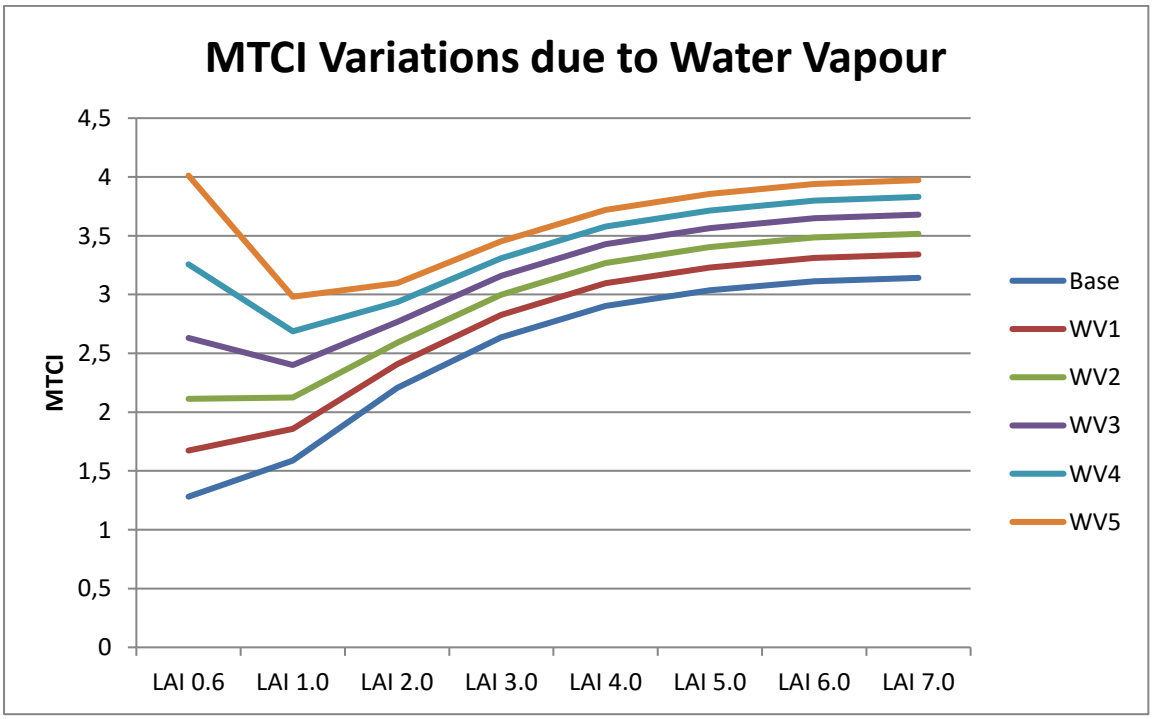

Figure 7: Reflectance fluctuations due to Water Vapour variations. Baseline has AOT=0; Water Vapour 0.01; Ozone 0.001 and Elevation 0.

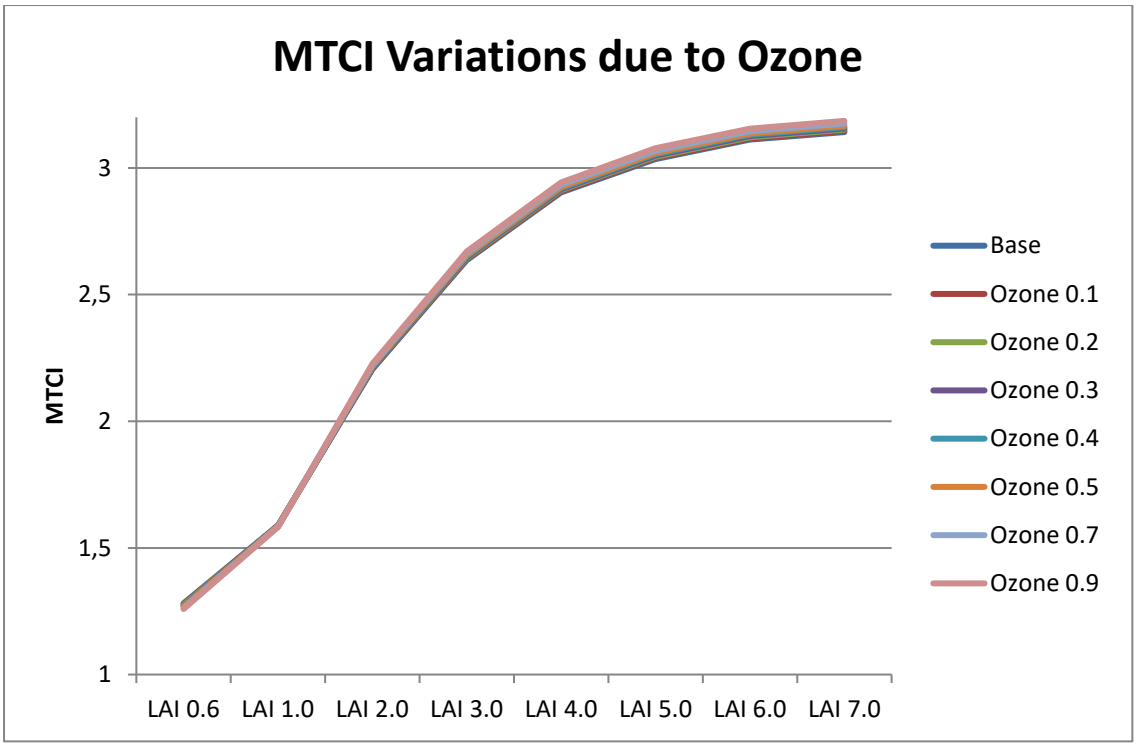

Figure 8: Reflectance fluctuations due to Ozone variations. Baseline has AOT=0; Water Vapour 0.01; Ozone 0.001 and Elevation 0.

Results indicate that an increase in water vapour content had very little impact on the apparent reflectance values in the red band of MERIS (see Figure 7). Increased AOT (Figure 6) results in an increase in apparent reflectance in the red band due to increased scattering of light in this portion of the EM spectrum by aerosol particles. An increase in Ozone (Figure 8) resulted in decreased levels of apparent reflectance in the red band. However, for the majority of results the change was very small and equated to a 6.5% reduction in reflectance at its most extreme (LAI 1.0 and Ozone 0.9). Results indicate that an increase in water vapour content caused a decrease in apparent reflectance in the red-edge band of MERIS. Increased AOT results in a gradual increase in apparent reflectance in the red-edge band due to increased scattering of light in this portion of the EM spectrum by aerosol particles. An increase in ozone results in decreased levels of apparent reflectance in the red-edge band. Results show that an increase in water vapour content had virtually no effect on apparent reflectance in the NIR band of MERIS. Increased AOT resulted in a gradual decrease in apparent reflectance in the NIR band due to increased levels of absorption of light in this portion of the EM spectrum by aerosol particles. An increase in Ozone resulted in decreased levels of apparent reflectance in the NIR band.

Overall, the effect of atmospheric conditions on MTCI values showed that an increase in water vapour content led to a substantial increase in MTCI values (see Table 9). Increased AOT resulted in a small increase in MTCI and an increase in Ozone resulted in a decrease of estimated MTCI values. These results are to be expected when considering the impact that different atmospheric conditions had on the component bands used for the MTCI calculation. Water vapour would be expected to increase the MTCI substantially as the Red and NIR bands remained largely unchanged but the apparent reflectance in the RE band decreased. AOT would be expected to increase the MTCI marginally as there was an increase in the apparent reflectance in the Red and RE bands and a decrease in the NIR band. Ozone would be expected to have the smallest effect on the estimated MTCI values as the apparent reflectance in all three component bands was found to decrease as the Ozone content increased.

Table 9: Absolute differences between Baseline MTCI and simulated MTCI. Negative numbers represent cases where the baseline MTCI was larger than the simulated MTCI – indicating a decrease in MTCI caused by the atmospheric parameter.

MTCI	LAI 1.0	LAI 2.0	LAI 3.0	LAI 4.0	LAI 5.0	Lai 6.0	LAI 7.0	Ave	St Dev
Base	1.5886	2.2063	2.6360	2.9031	3.0352	3.1121	3.1417	2.6604	0.5332
WV1	0.2696	0.2012	0.1916	0.1938	0.1956	0.1982	0.1990	0.2070	0.0257
WV2	0.5366	0.3848	0.3625	0.3652	0.3684	0.3730	0.3744	0.3950	0.0582
WV3	0.8121	0.5605	0.5231	0.5255	0.5293	0.5358	0.5378	0.5749	0.0975
WV4	1.0987	0.7291	0.6736	0.6744	0.6784	0.6865	0.6889	0.7471	0.1446
WV5	1.3929	0.8910	0.8168	0.8157	0.8199	0.8294	0.8322	0.9140	0.1970
AOT01	0.0008	0.0021	0.0030	0.0036	0.0039	0.0040	0.0041	0.0031	0.0011
AOT03	0.0160	0.0431	0.0623	0.0748	0.0811	0.0849	0.0864	0.0641	0.0242
AOT05	0.0295	0.0848	0.1242	0.1499	0.1630	0.1706	0.1736	0.1279	0.0495
AOT07	0.0416	0.1265	0.1875	0.2275	0.2478	0.2597	0.2643	0.1936	0.0766
AOT1	0.0588	0.1963	0.2965	0.3627	0.3962	0.4157	0.4231	0.3070	0.1256
Oz 01	-0.0012	0.0019	0.0034	0.0041	0.0044	0.0045	0.0046	0.0031	0.0020
Oz 02	-0.0014	0.0045	0.0075	0.0088	0.0094	0.0096	0.0097	0.0069	0.0038
Oz 03	-0.0029	0.0062	0.0107	0.0126	0.0135	0.0138	0.0140	0.0097	0.0057
Oz 04	-0.0031	0.0088	0.0148	0.0174	0.0186	0.0190	0.0192	0.0135	0.0076
Oz0.5	-0.0030	0.0117	0.0192	0.0225	0.0241	0.0246	0.0248	0.0177	0.0095
Oz 07	-0.0048	0.0157	0.0261	0.0307	0.0328	0.0336	0.0339	0.0240	0.0132
Oz 09	-0.0053	0.0206	0.0340	0.0400	0.0427	0.0437	0.0442	0.0314	0.0169

Uncertainty estimates

Using the baseline MTCI values as an assumed atmospherically corrected data set and comparing this with the simulated MTCI values revealed average uncertainty levels for MTCI values. Table 10 displays the results of the uncertainty analysis. Results indicated that average uncertainty was largest for data affected by water vapour (8.5 – 29.7% uncertainty). Water vapour uncertainty was largest for smaller LAI values and decreased as the LAI values increased. AOT had a smaller uncertainty level and the average continental AOT of 0.3 had an average uncertainty of 2.3%. Ozone had a very small level of uncertainty on MTCI values. The most typical continental ozone concentration is 0.3 and this had an average uncertainty of 0.3%. Ozone uncertainty increased as LAI increased.

Table 10: Percentage difference between Baseline MTCI and simulated MTCI. Negative numbers represent cases where the baseline MTCI was larger than the simulated MTCI – indicating a decrease in MTCI caused by the atmospheric parameter.

MTCI	LAI 1.0	LAI 2.0	LAI 3.0	LAI 4.0	LAI 5.0	Lai 6.0	LAI 7.0	Ave	St Dev
Base	1.5886	2.2063	2.6360	2.9031	3.0352	3.1121	3.1417	2.6604	0.5332
WV1	16.973	9.120	7.268	6.674	6.446	6.368	6.333	8.455	3.595
WV2	33.777	17.441	13.753	12.581	12.136	11.986	11.918	16.227	7.389
WV3	51.119	25.403	19.844	18.100	17.438	17.218	17.117	23.748	11.498
WV4	69.162	33.043	25.554	23.230	22.352	22.060	21.927	31.047	15.980
WV5	58.018	32.202	25.855	23.792	23.002	22.736	22.616	29.746	11.960
AOT01	0.050	0.095	0.113	0.123	0.127	0.130	0.130	0.110	0.027
AOT03	1.007	1.955	2.365	2.577	2.673	2.726	2.749	2.293	0.585
AOT05	1.860	3.843	4.711	5.163	5.369	5.482	5.527	4.565	1.232
AOT07	2.620	5.732	7.114	7.837	8.164	8.344	8.412	6.889	1.948
AOT1	3.699	8.896	11.246	12.494	13.052	13.359	13.467	10.888	3.291
Oz 01	-0.079	0.086	0.130	0.142	0.145	0.145	0.145	0.102	0.076
Oz 02	-0.086	0.206	0.284	0.304	0.310	0.308	0.309	0.233	0.135
Oz 03	-0.180	0.280	0.404	0.435	0.446	0.444	0.446	0.325	0.214
Oz 04	-0.196	0.398	0.560	0.600	0.614	0.612	0.612	0.457	0.276
Oz0.5	-0.189	0.529	0.727	0.776	0.793	0.790	0.790	0.602	0.335
Oz 07	-0.303	0.709	0.989	1.059	1.082	1.078	1.080	0.813	0.472
Oz 09	-0.334	0.935	1.290	1.379	1.408	1.405	1.407	1.070	0.594

Effect of AOT

AOT was found to cause an increase apparent reflectance in the Red and Red-edge bands and to cause a decrease in apparent reflectance in the NIR band. This was to be expected as Aerosols cause scattering in red light and absorption in NIR light (Karnieli et al. 2001; Van Leeuwen et al. 2006; Xiao et al. 2003). The effect was also greater in the red band than the red-edge or NIR bands which was expected as AOT effects are greater at shorter wavelengths where aerosol particle sizes are similar to EMR wavelengths (Kaufman and Tanre 1996). Since the RE band is very close to the red portion of the EM spectrum this would be expected to react to AOT in a way more similar to red than NIR light. Overall, an increase in AOT leads to a small increase in the estimated values of MTCI which is opposite to the effect on NDVI observed in Van Leeuwen et al. (2006) who found that NDVI decreased due to atmospheric aerosols. Van Leeuwen et al. (2006) also found that the reduction in NDVI values due to aerosols was larger for higher AOT and NDVI values. This was replicated in this study as changes in estimated MTCI were larger for higher AOT and LAI values. Thus, low NDVI and MTCI values appear to be less affected by AOT than high values.

Effect of Ozone

Red bands were expected to be affected by Ozone absorption the most followed by red-edge and NIR. Van Leeuwen et al. (2006) found that red reflectance was affected by ozone absorption, resulting in a decrease in apparent reflectance and that NIR was virtually unaffected by ozone absorption. Results for MTCI analysis revealed a different trend. Ozone absorption appeared to affect all three MTCI bands. For ozone concentrations of 0.1 – 0.3 the red band had the largest decrease in apparent reflectance followed by the red-edge and the NIR with the lowest. However, for ozone concentrations of over o.4 the NIR and Red-edge bands had significantly larger decreases in apparent reflectance than the red band. However, the effects were very small and standard uncertainties were typically less than 1% for ozone.

Effect of Water Vapour

Van Leeuwen et al. (2006) found that there was virtually no change in the estimated NDVI for different levels of atmospheric water vapour. However, estimated MTCI values increased substantially as water vapour increased. This difference between NDVI and MTCI was because NDVI uses only the red and NIR bands and neither of these is affected by water vapour. However, MCTI uses the RE band which was found to decrease due to water vapour (Figure 9). This decrease in RE and no change in red and NIR leads to an overall increase in the estimated MTCI values.

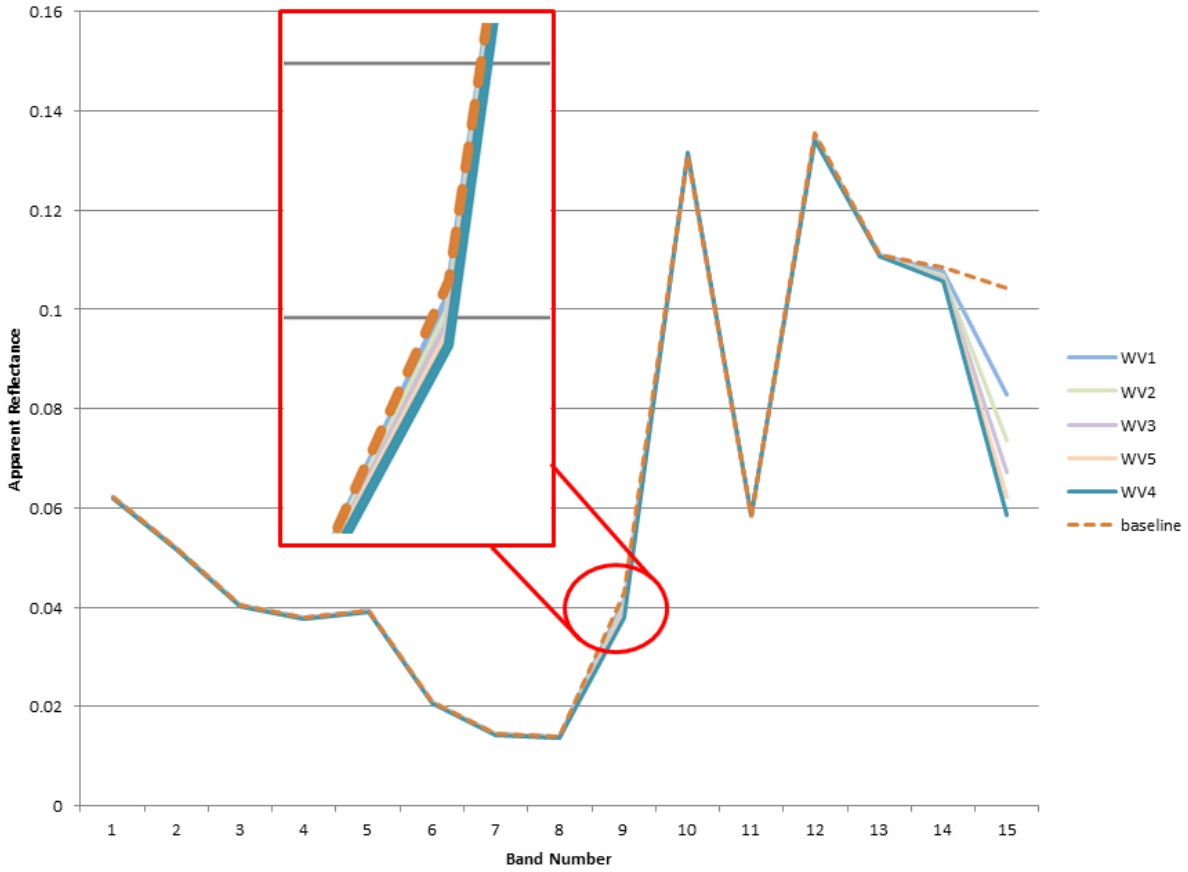

Figure 9: Effect of water vapour on red-edge band.

It is not clear why the RE band is affected by water vapour in this way. However, it could be that the RE band is positioned very close to a small water vapour absorption feature (Figure 10). This absorption feature could reduce the apparent reflectance in the RE band which would cause the decreased MTCI values seen in the MODO results. This could be further supported by the fact that Gons et al. (2004) indicated that changing the position of band 9 from 705 nm to 708.75 nm could have a significant "…influence [on] Chl a retrieval… because the absorption coefficient of water increases by >10% in this interval" (p 126).

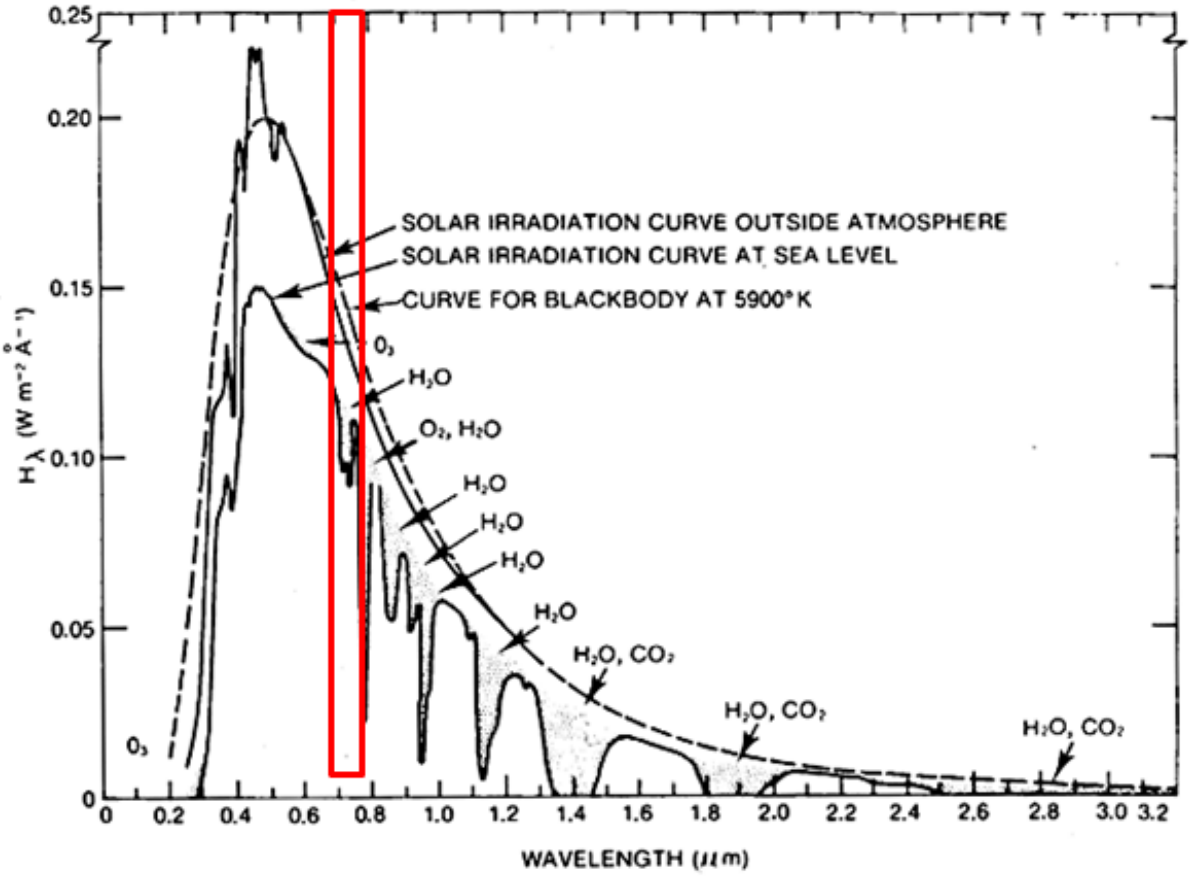

Figure 10: Location of small water vapour absorption band near to the RE band of MERIS.

6.6.2.2 Effect of data processing

Pixel values can vary depending on the processing chain used to estimate MTCI values. The most common difference in data processing is the use of differing atmospheric correction algorithms. Many different atmospheric correction algorithms are available for MERIS data. To explore the potential difference in MTCI values three different data processing chains (standard L2 BOA vegetation, SMAC processing and ATCOR-2 processing) were compared as part of this project. The study found that the majority of differences occurred in pixels with transparent cloud coverage or in areas with low levels of vegetation coverage. L2 and SMAC produced very similar per pixel estimations of MTCI (r^2 values ranged from 0.94 to 0.97). However, using ATCOR-2 for atmospheric correction resulted in significant differences in MTCI values as compared to those estimated using L2 and SMAC values. No ground truth data was available for this analysis and therefore no conclusions could be drawn as to which of the three methods (L2, SMAC and ATCOR-2) provided the most accurate MTCI estimation.

The ATCOR-2 approach requires the user to input several parameters that the L2 and SMAC do not require (for example, elevation, type of aerosol, and visibility estimates). In the experience of the MTCI-EVAL project ATCOR-2 produced accurate estimates of MTCI (as compared to ground data). However, the amount of supplementary data and the computer processing power required makes the ATCOR-2 approach inappropriate when large numbers of scenes are to be corrected. Therefore, the experience of the MTCI-EVAL project suggests that ATCOR-2 is useful for smaller scale regional analysis using a small number of scenes for processing. Thus, it is recommended that ATCOR-2 is not used for global scale analyses in its current guise and a more automated approach such as SMAC within the BEAM software could be used as it is much quicker to process imagery, providing a simplified but effective atmospheric correction and requiring less input data from the user.

6.6.2.3 Effect of Soil background brightness

The effects of soil background on OTCI showed that there was no significant effect of soil water content or soil type on the OTCI. However, in areas of sparse vegetation cover and high spatial heterogeneity of land cover types OTCI values were often high compared to values of NDVI for the same areas. This result led to the development of a soil flag. The extent of the influence of the soil was dependent on the coupled effect of the soil background reflectance with the

transmittance properties of the canopy. Figure 11 shows the trend of the standard uncertainty (Section 7 and AD 4) on the OTCI from low (1.5) to high (5.0) values. The peak at an OTCI value of between 2.0 and 2.5 confirmed the increase of uncertainty which was already experimentally observed in real data and which is due to the interaction between soil and vegetation at low vegetation cover.

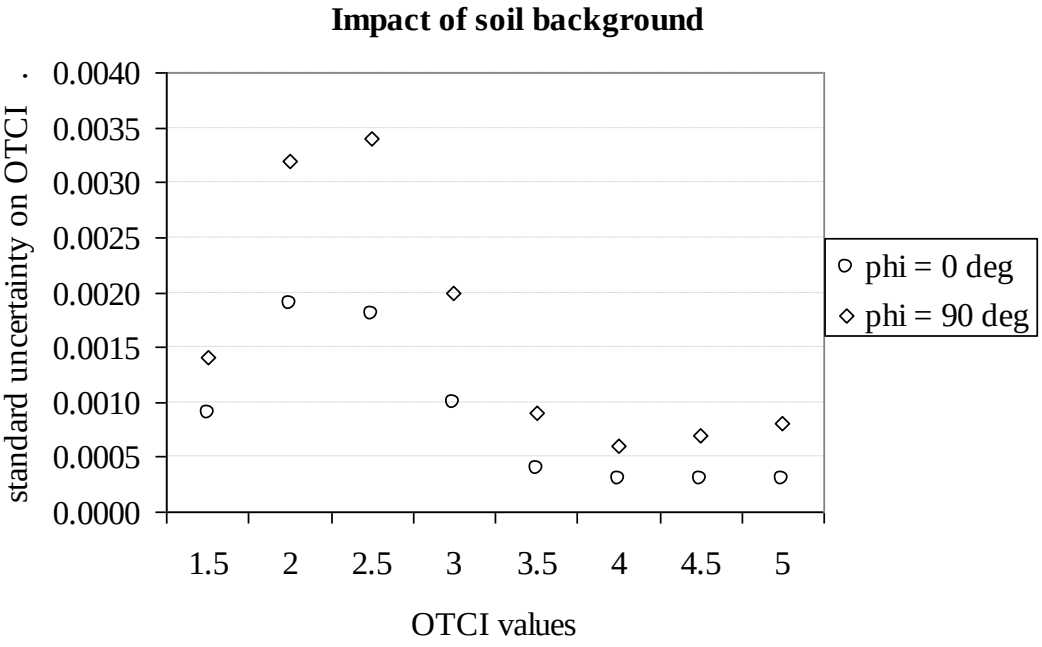

Figure 11: Impacts of different soil backgrounds

6.6.2.4 Effect of View angle

An inter-comparison between the SAILH and the FLIGHT model was carried out to test the correct geometry input and to verify the capability of the two radiative transfer models to reproduce the vegetation BRDF under similar canopy conditions (LAI=2.88; Leaf Chlorophyll=55, Leaf Angle Distribution=57 deg). Additionally, the FLIGHT model was set up to reproduce a one-dimensional canopy with 100% fraction of vegetation cover. The same soil reflectance spectrum was used for the two models. The analysis was carried out in the principal plain (difference between view and illumination azimuth angles was equal to 0 or 180 deg) and the Sun zenith angle was fixed at 30 deg. Figure 12 displays the reflectance in band 8, 9 10 and OTCI values for the SAILH and FLIGHT models used for this analysis.

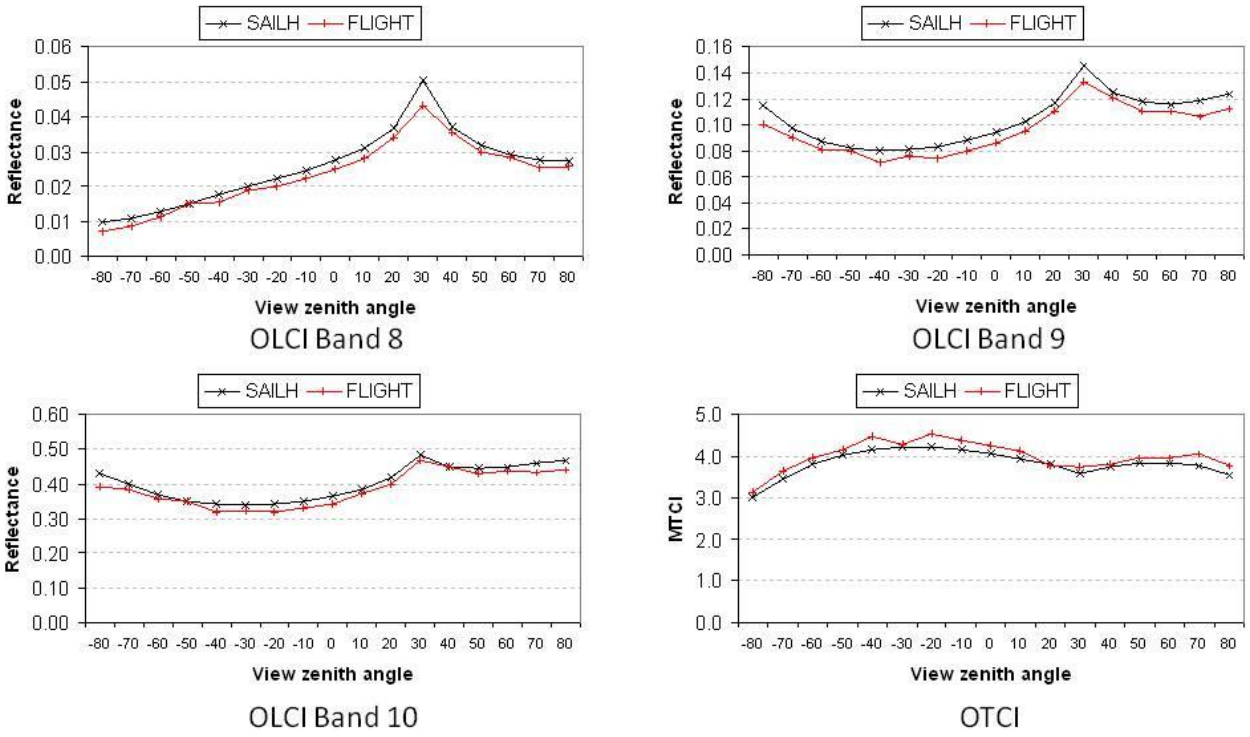

Figure 12: Showing the relationships between reflectance from the SAILH and FLIGHT models for OLCI bands 8, 9, 10, and OTCI.

The analysis demonstrated that the two models were able to reproduce the canopy BRDF across the principal plain and performed in a similar way when the same input vegetation parameters were used. The maximum percentage difference between the two models occurred at a view zenith angle of -80 deg and was equal to 30%, 13% and 10% for band 8, 9 and 10 respectively (Figure 13). The OTCI value was also given and had a maximum difference of 7% at – 40 degrees and an average difference of 4%.

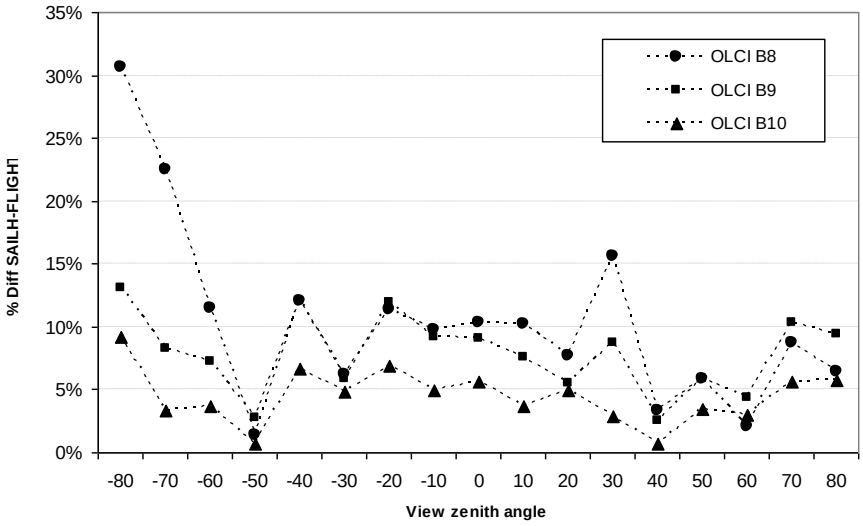

Figure 13: Percentage difference between SAILH and FLIGHT models in MERIS band 8, 9 and 10.

The impact of the satellite viewing angle acquisition at different latitudes emphasized only the effect of the view angle across transects from west to east relative to the image swath. Thus, the input geometry (Sun zenith and azimuth and view zenith and azimuth angles) to the canopy reflectance model was parameterized according to the full swath of the MERIS acquisition geometry along 12 different transects positioned from the North to the South hemisphere (70 N to 40 S at 10 deg steps). Results are provided in Figure 14. For the same MTCI value, a data series on the graph represent the standard uncertainty [AD 4] due to viewing angle (due to satellite swath) for a given combination of Solar Zenith Angle (SZ) and Solar Azimuth (SA) angle.

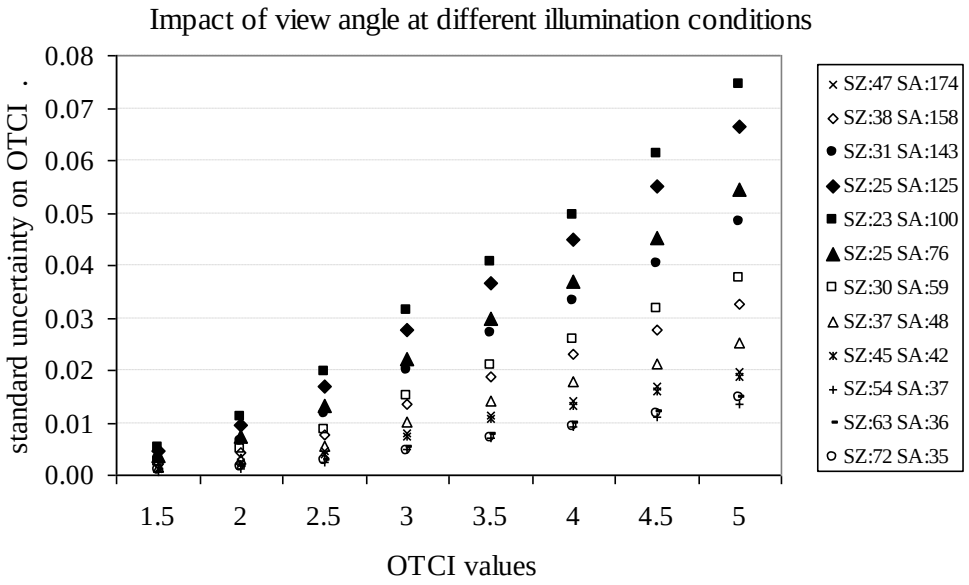

Figure 14: Impact of view angle at different latitudes under different illumination conditions

The setup of the OLCI on Sentinel-3 will be very similar to MERIS with the exception of the view angle as OLCI cameras will be tilted about 12 degrees across-track away from the Sun to avoid sun-glint effects. Due to the close similarity between the two sensors the error propagation calculation analysis was conducted on the MERIS sensor and applied to the OLCI.

However, the change in camera tilt will produce a difference in the viewing angle between the two data sets for a given location and swath position. An example of the view angle across transect for a given image swath is given for MERIS and the equivalent OLCI Sentinel-3 data (Figure 15).

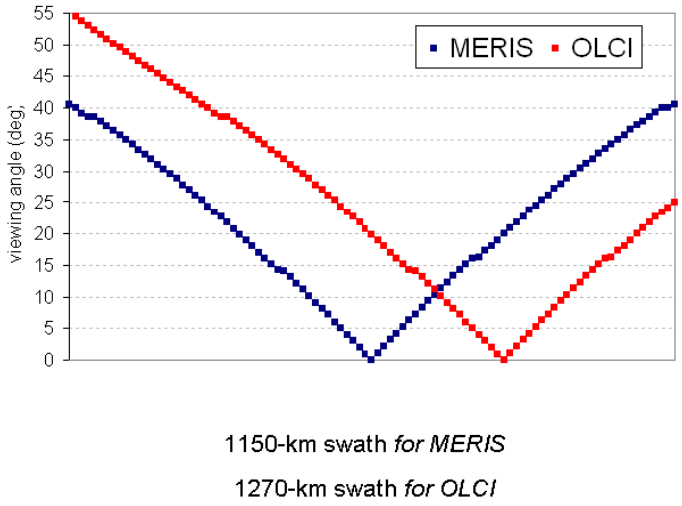

Figure 15: For a given MERIS acquisition the graph reports the view angle across transect on the swath and the equivalent OLCI viewing angle for a given location.

The spectral reflectance of reduced resolution (RR) MERIS L2 data was extracted from selected pixels and used in model inversion (PROSAILH model in inverse mode) to estimate canopy variables. Retrieved canopy variables were used to simulate reflectance (PROSAILH model in forward mode). MTCI was calculated for given locations according to MERIS geometry and corresponding OLCI viewing angle estimated as in Figure 16. MTCI values for two cases are presented with the relative difference (as a percentage) between OLCI and MERIS. For the two cases considered, the differences ranged between 0.35% and 5.3% with a mean relative difference of 2.3%.

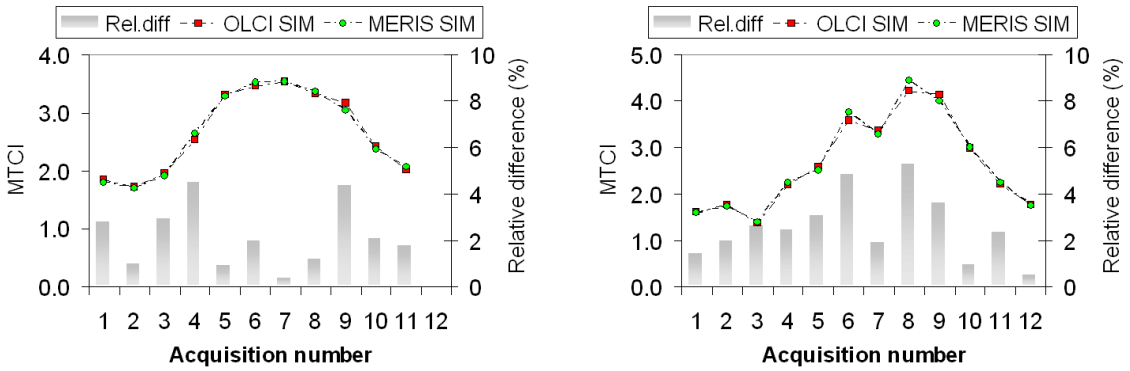

Figure 16: The green dots represent the MTCI simulated according to the MERIS geometry for each of the 12 acquisitions. The red dots represent the MTCI simulated according to MERIS geometry and corresponding OLCI viewing angle. The grey bar indicates the absolute relative difference (%) between the two MTCI simulated values.

An example of the total uncertainty per pixel for the entire view angle range is provided for two combinations of SZA and SAA angles and for a range of OTCI values. The two combinations of SZA SAA provided the minimum (SZA:38 SAA:158) and the maximum (SZA:23 SAA:100) error, in Figure 17 and in Figure 18 respectively.

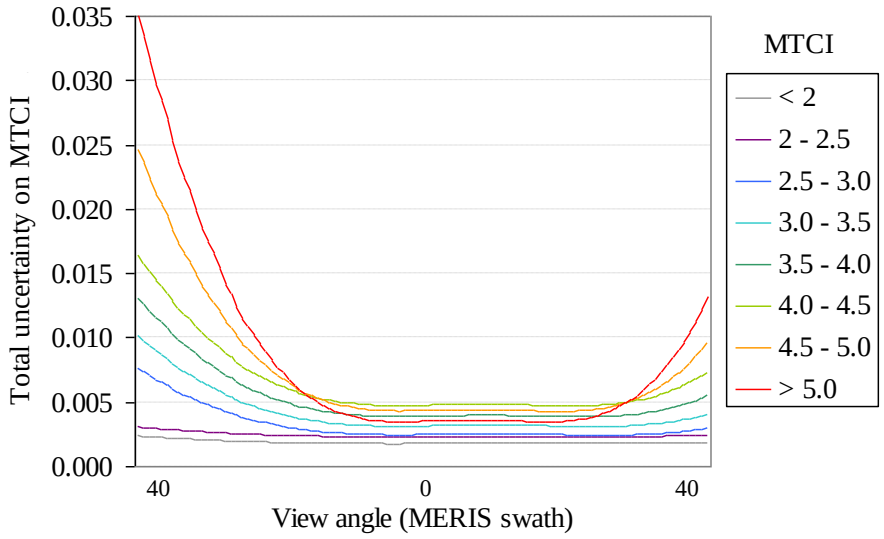

Figure 17: Total uncertainties on MTCI or OTCI for a SZA of 38 degrees and a SAA of 158 degrees

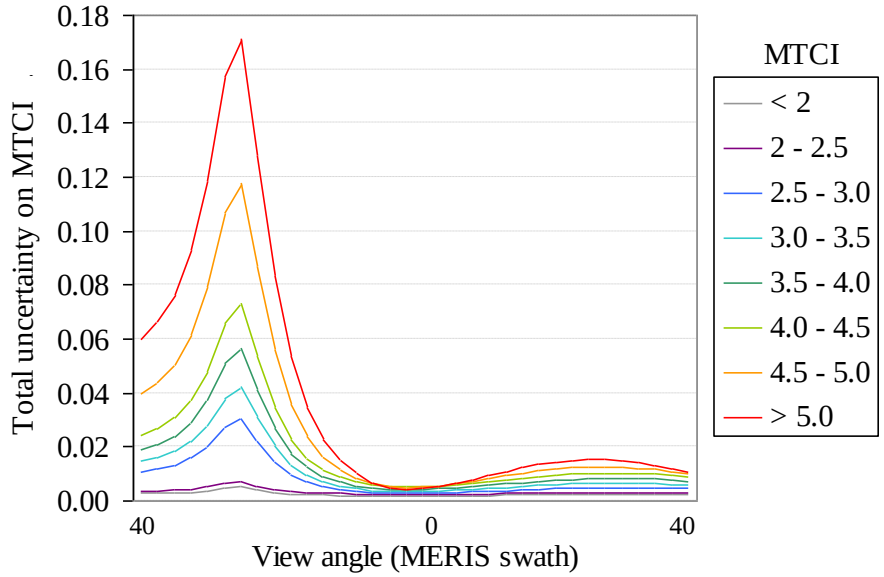

Figure 18**: Total uncertainty on MTCI or OTCI for a SZA of 23deg and a Sun Azimuth angle of 100 deg**

6.6.2.5 Effect of random noise

Acquisition noise due to detector quality and calibration uncertainty with no correlation between bands was considered. The total error on the OTCI due to adding from 2% to 4% uniformly distributed random noises was estimated as this would be the average noise expected from the OLCI instrument and results are presented in Figure 19.

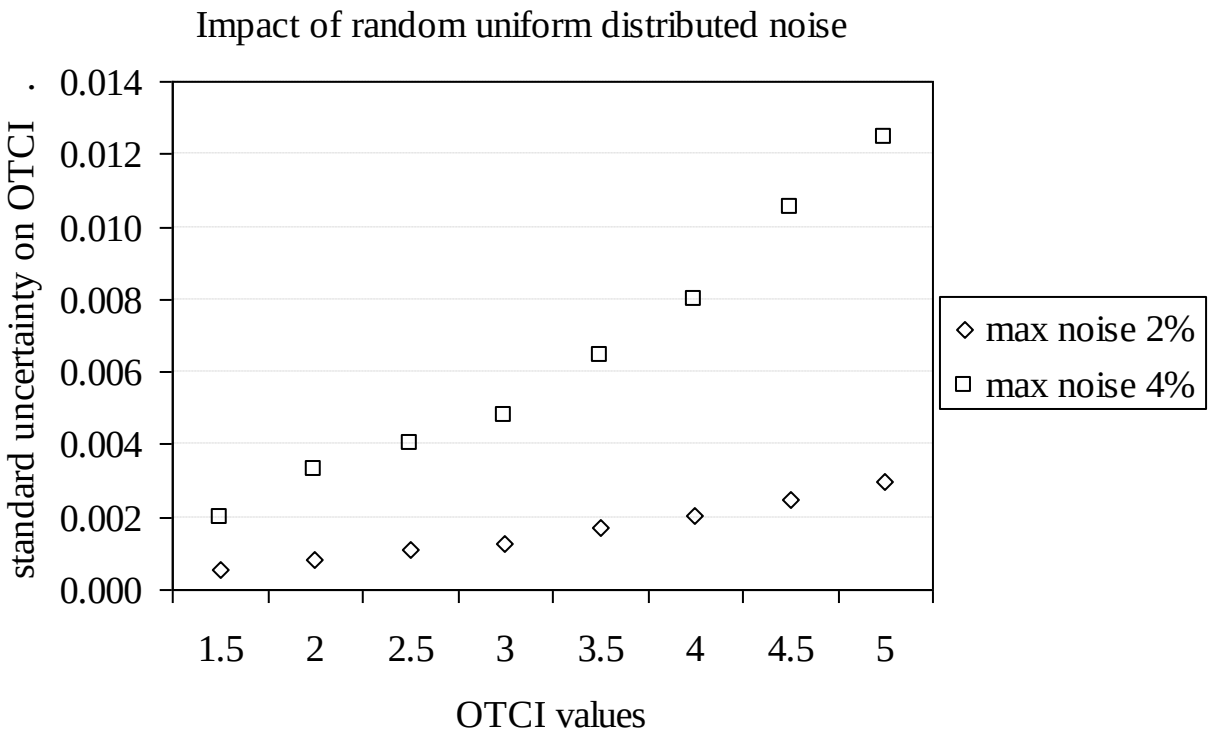

Figure 19: Impact of instrument noise on the OTCI. The noise is calculated as random standard distribution with two different maximum levels: 2% and 4%.

6.6.3 *Accuracy assessment*

At the moment we cannot precise the maximum size of LUT (the optimal resolution of the LUTs (SZA, VZA and OTCI values)) that can be used in the operational implementation. Before finalising the LUT we will need to investigate what is the maximum possible size of LUT that can be accepted in the operational implementation. The size of the LUT and the computational requirement will be considered in defining the final resolution of the LUT. At this time we are considering a resolution between 1 and 10 deg for the geometry and 0.25 - 6.5 for OTCI values.

This is because we want to consider the variance of the uncertainty with in different geometric interval. For example, if between 1 degree and 10 degree the variation is minimum the resolution of the LUT would be 10 degrees to speed up the processing.

The results of the analysis of error propagation across the entire range of MTCI/OTCI are summarized in Table 11.

Table 11: Error propagation results for the entire range of MTCI

Error source	Min error	Max error
Acquisition noise	0.002	0.0124
Illumination and view geometry	0.0008	0.0745 (~ 7%)
Soil background	0.0003	0.0034

There will be three different flags for the OTCI:

- OTCI Flag for bad data which will include spectral tests and an OTCI range to avoid bad pixels and saturation;
- OTCI Flag for soil background effects, and;
- OTCI flag for the view zenith and solar zenith angle (geometry flag).

If the pixel in question meets all of the criteria for the flags an OTCI value will be calculated with an associated uncertainty. Note that the uncertainty will include geometry, noise and soil effect.

6.7 Assumptions

The following assumptions were made in the design of the OTCI algorithm:

- All water pixels masked prior to estimation of OTCI:
- Non-saturated OLCI level 2 normalised surface reflectances are available in 681nm, 708 nm and 753nm spectral bands;
- Positive Level 2 normalised surface reflectances are available in 681nm, 708 nm and 753nm spectral bands;
- Level 2 normalised surface reflectances are used as input corrected for the seasonally variable distance between the Earth and Sun;

- OTCI values more than 6.5 set to 0;
- Adjacency effects are ignored, and;
- Substantial atmospheric aerosol loads, as observed in dust storms and heavily polluted areas are screened out.

7 Error Assessment Description

A standardised method was selected to conduct the validation and sensitivity analysis for the MTCI and the proposed chlorophyll indices from Sentinel-3. The 'Guide to the Expression of Uncertainty of Measurement' (GUM) provides general guidance on aspects of the stages of uncertainty evaluation. The Quality Assurance framework for Earth Observation (QA4EO) was formed to help establish common quality guidelines for Earth observation. The QA4EO devised an operational framework that stipulates that all data and information products derived from Earth observation sould have quality indicators (QIs) associated with them. These QIs should enable all users to understand a products fitness for a specific purpose. Within the ten guidelines that have been devised by the QA4EO the "*A guide to expression of uncertainty measures"* [AD 4] has been followed during this study.

Expression of uncertainty measurements includes several "stages" required to evaluate the uncertainty contained in the data and information products. These stages include;

- The definition of the quantity to be measured (Y) for example, the chlorophyll content of a canopy;
- Specific input quantities (X_i) which the Y will depend, for example, the spectral reflectance in band 8, 9 and 10 of the MERIS sensor or bands 10, 11 and 12 of the OLCI Sentinel -3 sensor would be represented by X_1, X_2, X_3 ;
- A model is then developed to relate the output (Y) to the inputs (X_i), in the form of y = f(x), Thus, for example, the MTCI equation provides a way of modelling a series of MERIS bands (x_i) to produce an estimate of MTCI (Y):

$$MTCI = \frac{R_{band10} - R_{band9}}{R_{band9} - R_{band8}} = \frac{R_{753.75} - R_{708.75}}{R_{708.75} - R_{681.25}}$$

Equation 3

- Using the probability density functions (PDFs) of the values of Xi can obtain a PDF for the value of Y;
- Using the PDF of the output (Y), the best estimate of the output the standard uncertainty, u(y) of the best estimate of Y can be obtained and reported.

Operational use of MTCI requires detailed understanding of the limiting factors and quantification of uncertainties due to sensor calibration noise, soil background changes, varying

viewing and sun angle configuration and atmospheric influence. The impact of these factors on the calculation of the MERIS MTCI and the Sentinel-3 TCI were evaluated and total uncertainty ascertained. The approach to model the propagation of uncertainties was based on the law of propagation of uncertainty as described in Miura et al. (2000) [RD 46]. Model based Top of Canopy (TOC) reflectance for a range of vegetation characteristics, soil background, acquisition geometries and sensor noise was considered for this analysis. The analysis was based on the estimation of the MTCI (see equation 3) and the TCI for sentinel-3 were calculated using bands that corresponded to those on MERIS. The MTCI was generated for different view angles, soil conditions and data noise.

The law of propagation of uncertainty denoted by μ(MTCI), estimates the standard uncertainty of the MTCI from the standard uncertainties of the input reflectance's in NIR, red edge and red spectral bands (denoted by $\mu(\rho_{NIR})$, $\mu(\rho_{rededge})$ and $\mu(\rho_{red})$). The uncertainty was based on the partial derivatives of the relationship between MTCI and surface reflectance in NIR, red edge and red spectral bands. The uncertainty propagation in Equation 4 is based on a first order Taylor series approximation of the MTCI calculation (Equation 3).

$$\mu^2(MTCI) = \left(\frac{\partial MTCI}{\partial \rho_{NIR}}\right)^2 \mu^2(\rho_{NIR}) + \left(\frac{\partial MTCI}{\partial \rho_{rededge}}\right)^2 \mu^2(\rho_{rededge}) + \left(\frac{\partial MTCI}{\partial \rho_{red}}\right)^2 \mu^2(\rho_{red}) + 2\frac{\partial MTCI}{\partial \rho_{NIR}}\frac{\partial MTCI}{\partial \rho_{red}} * \mu(\rho_{NIR}\rho_{red}) + 2\frac{\partial MTCI}{\partial \rho_{NIR}}\frac{\partial MTCI}{\partial \rho_{rededge}} * \mu(\rho_{NIR}\rho_{rededge}) + 2\frac{\partial MTCI}{\partial \rho_{rededge}}\frac{\partial MTCI}{\partial \rho_{red}} * \mu(\rho_{rededge}\rho_{red}) \quad \text{(Equation 4)}$$

Where:

$$\left(\frac{\partial MTCI}{\partial \rho_{NIR}}\right)^2 \mu^2(\rho_{NIR}) = \left(\frac{1}{\rho_{rededge} - \rho_{red}}\right)^2 * \mu^2(\rho_{NIR}); \quad \text{(Equation 5)}$$

$$\left(\frac{\partial MTCI}{\partial \rho_{rededge}}\right)^2 \mu^2(\rho_{rededge}) = \left(\frac{\rho_{red} - \rho_{NIR}}{(\rho_{rededge} - \rho_{red})^2}\right)^2 * \mu^2(\rho_{rededge}); \quad \text{(Equation 6)}$$

$$\left(\frac{\partial MTCI}{\partial \rho_{red}}\right)^2 \mu^2(\rho_{red}) = \left(\frac{\rho_{NIR} - \rho_{rededge}}{(\rho_{rededge} - \rho_{red})^2}\right)^2 * \mu^2(\rho_{red}); \quad \text{(Equation 7)}$$

Uncertainty was reported first for individual factors affecting the accuracy or uncertainty and then the uncertainty due to the combination of factors.

7.1 Quality Flags Description

Quality control is essential to define robust and reliable biophysical products from satellite data. Two major factors affect the quality of the retrieval of biophysical variables: (i) problems with input data (for example, L1b) and (ii) conditions with satellite observations which make the retrieval of biophysical variables unreliable (for example, atmospheric conditions or high sun viewing angles). Some of these factors may be generic and may affect most of the biophysical variable retrieval algorithms, whereas some factors may be specific to particular biophysical variables. Therefore, most of the operational biophysical products come with the respective quality indicator.

Each OTCI pixel value will be associated with a quality flag pixel. The quality flag pixel will be an 8-bit flag and the resulting value will be provided as an integer. The flag will mainly consider the effects of overall data quality, angular effects, aerosol and soil. The 8-bit flag details are provided in Table 12. Each aspect of the overall quality flag will be associated with a flag concerned with each individual aspect of data quality; (i) bad data; (ii) view angle; (iii) aerosols, and; (iv) soil. These flags are described in more detail in the subsequent sections.

Table 12: OTCI Quality Flag details

Quality Flag	Data	Angular effect	Aerosol	Soil effect
Description	Data quality/spectral test/ cloud/snow	Combination of both sun and sensor view angle	Flag out areas of high aerosol (currently no data)	Identify pixels where soil effect is dominant
Bit position	8,7	6,5	4,3	2,1

7.1.1 *OTCI flag for bad data*

Pixel classification generally provides three outputs: land, water and cloud/snow/bright pixel. Within the land class we need to have a spectral test within the internal processing of OTCI to check if the land pixel is suitable for OTCI estimation. The following spectral tests should be performed to identify invalid input data:

OTCI:

- Normalised surface reflectance in band number 10 (*p*red) <= 0;
- Normalised surface reflectance in band number 10 (*p*red) >= 0.3;
- Normalised surface reflectance in band number 12 (*p*NIR) <= 0.1;
- Difference between band number 12 and band number 10 (*p*diff1) < $1*10^{-6}$; and
- Difference between band number 17 and band number 10 (*p*diff2) >= 0.05.

MTCI (4RP):

- Normalised surface reflectance in band number 8 (*p*red) <= 0;
- Normalised surface reflectance in band number 8 (*p*red) >= 0.2;
- Normalised surface reflectance in band number 10 (*p*NIR) <= 0;
- Normalised surface reflectance in band number 10 (*p*NIR) <= 0.1;
- Difference between band number 10 and band number 8 (*p*diff1) < $1*10^{-6}$; and
- Difference between band number 13 and band number 8 (*p*diff2) >= 0.05.

The pixel-based check is internal and an integral part of the algorithm and should be done before calculating OTCI. If input data are valid, a final pixel-based check will be performed to verify that OTCI values are within the possible OTCI range. The data quality flag is set out in Table 13.

Table 13: Quality flag description for bad data

		Pixel Quality	Description
1	1	Very good	No cloud, passed the spectral test, good data quality
0	0	Poor	Cloud/failed the spectral test/ bad quality data

The verification of the range limits for OTCI will require externally derived coefficients for upper and lower limits (two 2 scalars, fixed values):

- OTCI Range: Lower limit = >0; Upper limit = 6.5.

The range suggested for the OTCI is slightly larger than implemented for MTCI in the 3th Reprocessing (MTCI range 0 - 5.5) because research suggested that the range could be increased from 5.5 to 6.5 without increasing the probability of including saturated pixels.

7.1.2 *OTCI flag for view angle*

Acquisition geometry uncertainty calculation will be based on model data (pre-computed) and will be applied for each pixel by using information stored in a Look-up-Table (LUT). For a discrete combination of SZA and VZA, the table will provide per pixel maximum uncertainty values as function of OTCI values (in discrete classes, i.e., for 1.5<OTCI <2.0, for 2.0<OTCI <2.5).

Considering an OLCI scene for the j^{th} pixel, four main parameters will be required to identify OTCI uncertainty from the LUT:

- SZA(j^{th}): pixel-based Sun Zenith Angle;
- SAA(j^{th}): pixel-based Sun Azimuth Angle;
- VZA(j^{th}): pixel-based View Zenith Angle, and;
- OTCI(j^{th}): pixel-based OTCI values

The LUT can be implemented in a single LUT (one file) or two LUT (index table and pre-computed uncertainty table) files and description of the quality flag is given in Table 14.

Table 14: Quality flag description for view angle

			OTCI		MTCI (4RP)	
		Pixel Quality	VZA	SZA	VZA	SZA
1	1	Very Good	< 30˚	> 40˚	Default	
1	0	Good	30 < 40˚	> 30 ≤40˚	> 30 ⩽ 40°	> 40°
0	1	Fair	≥ 40 < 50˚	> 20 ≤ 30˚	⩽ 40°	⩽ 40°
0	0	Poor	≥ 50˚	≤ 20˚	> 40°	

7.1.3 *OTCI flag for Aerosol*

Since the effect of Aerosol Optical Thickness (AOT) correction is not proportional to wavelengths, even band ratio vegetation indices could still be affected by AOT to a certain extent. For the OTCI, this effect was quantified with about 2.9% at low AOT (AOT_{440} < 0.3) and 21.6% at very high AOT (AOT_{440} > 1.4). The combined error (from low to very high AOT) is however acceptable, with a relative RMSE of 6.4% compared to MTCI calculated after Aerosol correction.

Since the AOT algorithm output processing is not operationally implemented in OLCI L2 standard products, it cannot be exploited to provide AOT estimates and thus to quantify uncertainties related to OTCI calculation. However, depending upon the operational suitability it is proposed to have aerosol information from the OLCI-AATSR synergy product. At the moment to maximise data coverage the Aerosol flag is set to 1 (all good quality). However, if information on AOT is available then the following flag should be used (Table 15).

Table 15: Proposed Aerosol flag to be used if information on AOT is available

		Pixel Quality	AOT_{440}	Remark
1	1	Very good	<0.3	These thresholds are for indicative purpose and would require further investigation
1	0	Good	0.3-0.7	
0	1	Fair	0.7-1.4	
0	0	Poor	>1.4	

7.1.4 *OTCI flag for Soil*

The flag for soil will be identified using the Soil Discrimination index (SDI). The algorithm will require the OLCI spectral band number 12 (753.75 nm), 10 (681.25 nm) and 6 (560 nm) for the calculation of a soil flag according to the following formulation:

$$\text{Soil Discrimination Index} = \frac{\rho\text{NIR}/\rho\text{Red}}{\rho\text{Red}/\rho\text{Green}} \qquad \text{Equation 8}$$

The result of this equation will be compared for each pixel with an external threshold (1 scalar, fixed value 0.9) to classify pixels not adequate for OTCI calculation (e.g. bare soils or very sparse vegetation). The details of the soil flag are presented in Table 16.

Table 16: Soil flag description

		Pixel Quality	SDI Threshold	Land cover
1	1	Very good	≥0.9	Non-Soil
1	0	Good	≥0.9	Non-soil
0	1	Fair	<0.9	Soil
0	0	Poor	<0.9	Soil

7.1.5 *Quality flag file*

All the quality flags will be combined to provide one value (binary to integer conversion). Some examples are given in Table 17.

Table 17: Overall quality flag description

Flag value	Integer value	Description
11111111	255	Pixels are good quality, not affected by soil, view angle and aerosol (best quality data)
11101111	239	Pixels are good quality, not affected by soil and aerosol, but little affected by view angle (reasonable quality)
11101110	238	Pixels are good quality, not affected aerosol, but change of affected by soil and view angle (reasonable quality)
11001111	207	Pixels are good quality, not affected by soil and aerosol, but are severely affected by view angle
11001110	206	Pixels are good quality, not affected aerosol, but are severely affected by view angle and change of soil effect
11001100	204	Pixels are good quality, not affected aerosol, but are severely affected by view angle and soil effect

7.2 Limitations

It has to be pointed out that the analysis conducted in this study explores the sensitivity of MTCI/OTCI solely on MERIS data sets. No simulated OLCI data was available during the project. Since the OLCI sensor is similar to the MERIS sensor in terms of spatial, spectral and radiometric specifications results for MTCI have been assumed to be representative of the OTCI data that will available from the OLCI sensor. However the OLCI sensor will be titled 12˚ and therefore, will have some differences with MTCI. Thus, the sensitivity analysis had only a demonstrative scope to show the possible differences between the two sensors under the hypothesis of coincident image swath. Similar or greater differences can occur between consecutive acquisitions with image centres that do not correspond to each other.

Chlorophyll content varies with the amount of chlorophyll in the vegetation and the amount of vegetation. If chlorophyll concentration is constant then change in LAI will change reflectance. Therefore, the effect of LAI on the MTCI estimation should be investigated. Many of the field campaign datasets used for this study were collected by third parties for different purposes and therefore, often no chlorophyll information was collected. When chlorophyll information was collected it was often not very varied and a large number of ESUs had very similar chlorophyll values. This effectively reduces the amount of data that is available for sensitivity analyses and validation.

During the study no ancillary data such as the content of ozone and water vapour, ground elevation or AOT were available. This lack of ancillary data led to two limitations of the study; (i) atmospheric correction procedures were not as accurate as they could have been with the data included, and; (ii) the exploration of the effect of atmospheric conditions on MTCI was not able to create baseline conditions that represented the reality of the conditions during the data collection period. In future, if atmospheric conditions were collected during the field campaigns atmospheric correction would be more accurate and the resulting TOC reflectance would be more closely matched to the ground spectra that were collected. Further, a more thorough examination could be conducted into the effect of atmospheric conditions on the estimation of MTCI. The absorption due to other leaf components, besides chlorophyll, such as several pigments that are contained in leaves and that absorb radiation in red wavelengths could alter MTCI independently of chlorophyll concentration. However it was assumed that this effect is not significant at a regional scale using MERIS sensor. Effect of absorption due to other leaf components on MTCI estimation has not been considered.

8 Validation Status

We have summarised briefly some of the results of the extended validation of MTCI/OTCI that was conducted since 2006. To validate MTCI and OTCI two main methodologies have been adopted. In first methodology, *in-situ* measurements of canopy chlorophyll content (CCC) collected within Elementary Sampling Unit (ESU) are upscaled using high resolution multispectral data (e.g. RapidEye, Sentinel-2). The upscaled map of the biophysical variable is then compared to the L2 product. The second methodology is based on the intercomparison between MTCI and OTCI to evaluate the consistency between the products. The following subsections present details of these methodologies and the main results.

8.1 Upscaling of field measurements for MTCI (4RP) validation

Direct validation of MTCI 4RP was conducted using in-situ canopy chlorophyll content (CCC) data collected in two previous field campaigns. One campaign was carried out between 11 July and 19 July 2006 in Southern England [RD 29], and the other one between 23 August and 25 August 2009 in Southern Italy [RD 30].

The first campaign was in Dorset, where a total of 8 fields covering 6 crops were sampled (beans, wheat, grass, linseed, maize and oats). The fields included diverse growing stages and canopy architecture. Within each field, Leaf area index (LAI) and leaf chlorophyll concentration (LCC) were collected at 3 to 5 elementary sampling units (ESU). LAI-2000 instrument was used to estimate LAI while LCC was estimated using the hand-held SPAD-502 chlorophyll meter. The MTCI 4RP scene for the validation was ENV_ME_2_FRG____20060718T105905_20060718T111150_____0765_049_309_____ACR_R_NT____.SEN3.

In the second field campaign, 36 ESU were sampled in an agricultural zone in the Campania region, Italy. Multiple fields were included such as alfalfa, maize, plum, apricot, kiwi, peach, aubergine, pepper and artichoke. At each ESU, 18 random estimations of LAI were recorded using the LAI-2000 and 30 random estimations of LCC were made with the SPAD-502 chlorophyll meter. Readings were averaged to produce a single mean value for LAI and LCC per ESU. For this campaign, an intermediate upscaling of the biophysical variables was carried out using multispectral data acquired on 17 August 2009 from the RapidEye mission. A high resolution reference map was generated by inversion of the coupled Leaf Optical Properties

Spectra (PROSPECT) and Scattering by Arbitrarily Inclined Leaves (SAIL) radiative transfer models (RTMs) using a look-up table (LUT). The reference map showed strong agreement with in-situ data (r = 0.87, RMSE = 0.39 g m^{-2}). Both, the high resolution biophysical map and the MTCI 4RP dataset were downscaled to a common spatial resolution of 1 km. The MTCI 4RP product employed in the validation exercise was: ENV_ME_2_FRG____20090817T092720_20090817T093802_____0642_081_394_____ACR_R_NT____.SEN3.

Figure 20a and Figure 20b show the agreement between in-situ CCC and MTCI 4REP for the England and Italy campaign, respectively. In both campaigns MTCI 4REP depicts a strongly linear relation to CCC (r=0.71; r=0.91).

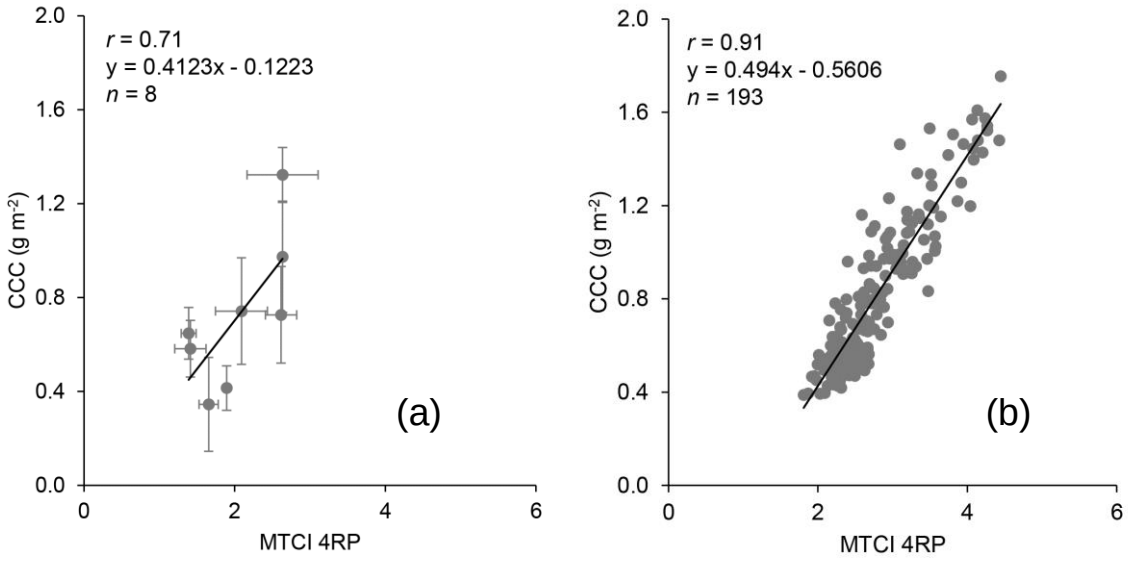

Figure 20: Comparison between CCC and the MTCI for the 4RP (a) Southern England and (b) Southern Italy campaigns.

8.2 Upscaling of flied measurements for OTCI validation

This section presents the validation of OTCI over a Mediterranean environment. The purpose of the study was to evaluate the ability of OTCI to estimate CCC and to investigate the use of Sentinel-2 (S2) Multispectral Instrument (MSI) in the upscaling process [RD 28]. A field campaign was conducted in the Valencia Anchor Station, Spain, in June 2017. The study site covered a relatively flat agricultural area of 10 km x 10 km dominated by vineyard. Ground measurements of LAI and LCC were collected at 32 ESU of 40 m x 40 m. LAI was derived from Digital Hemispherical Photography (DHP), the photographs were processed according to standard procedures that account for leaf clumping. To estimate LCC, SPAD-502 potable chlorophyll meter readings were converted to actual LCC using calibration functions.

A S2 scene acquired during the field campaign period was used to generate CCC reference maps. Two approaches were employed to compute these maps. In the first approach, artificial neural network (ANN) and radiative transfer model (4SAIL and PROSPECT-4) simulations were used to retrieve CCC. The second approach consisted on establishing an empirical relationship between CCC at the 34 ESU and the S2 Terrestrial Chlorophyll Index (S2TCI). Statistical metrics Pearson correlation coefficient and RMSE cross validation leave-one-out were used to evaluate the agreement and accuracy of the maps. The maps were then spatially aggregated or downsampled and collocated to match the grid and pixel size (300 m x 300 m) of a Sentinel-3A OTCI scene acquired during the time of filed campaign. Regression analysis was used to obtain an empirical equation between ESU CCC and OTCI, which was then used to regress CCC values. Similarly, retrieved CCC accuracy was evaluated through RMSE and NRMSE.
The results showed that CCC retrieved from the S2 dataset satisfactorily depicts the spatial distribution of OTCI for the study area (Figure 21). Quantitatively, correlation between upscaled CCC and OTCI is r=0.77 (Figure 22) and the empirical relationship is defined by:
$y=0.1452x+0.1191$
where y is CCC in $g*m^2$ and x represents OTCI.
The accuracy of the CCC estimated using the empirical equation above was high (RMSEcv=0.02 $g*m^2$; NRMSEcv=5%) (Figure 22). These results indicate that OTCI realistically relates to *in-situ* CCC and highlights the utility of red-edge bands of S2, that enable the computation of OTCI-like index, for upsacaling of ground measurements.

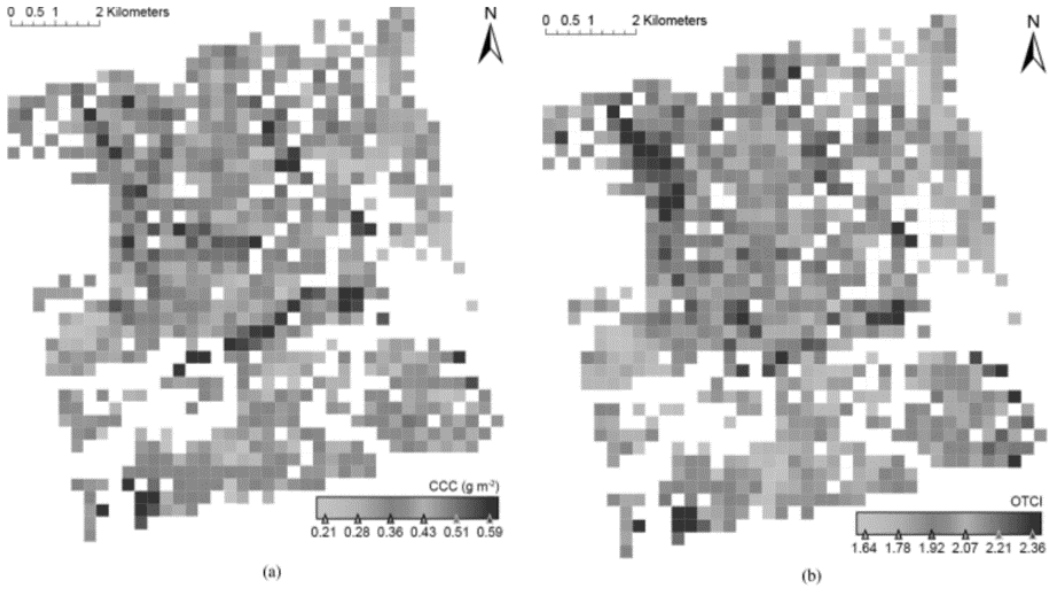

Figure 21: (a) 300-m CCC reference map derived using mean value downsampling and (b) OTCI (areas not covered by considered land cover types masked). Reproduced from [RD 28].

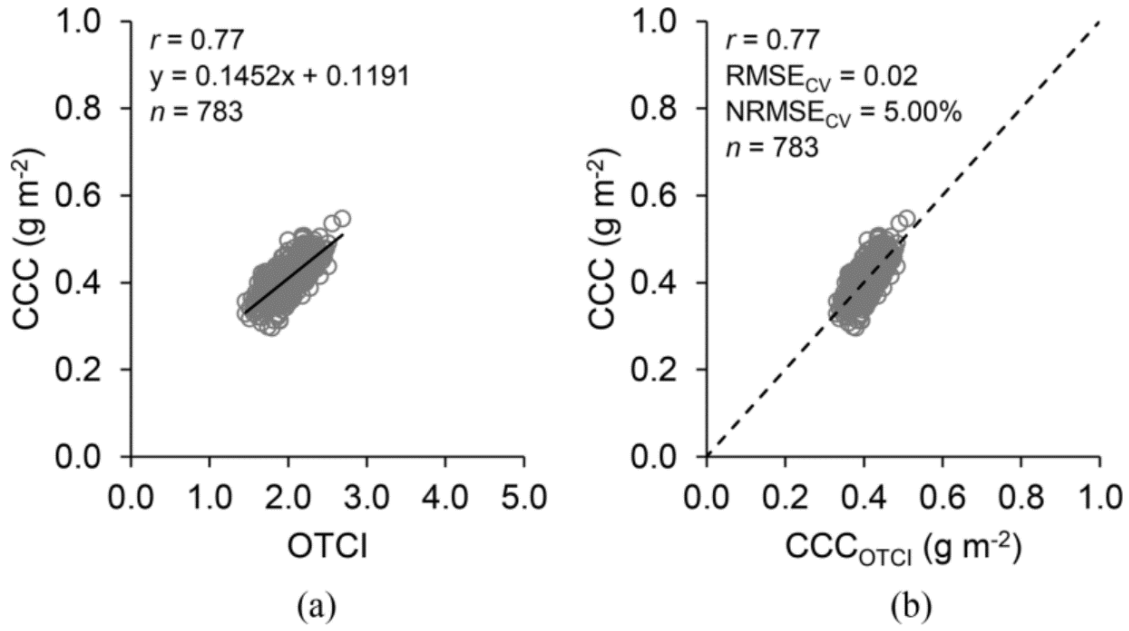

Figure 22: Comparison between upscaled CCC and the (a) OTCI and (b) OTCI-based CCC retrievals. The solid line (a) represents the established empirical relationship (7) whilst the dashed line (b) represents a 1:1 relationship. Reproduced from [RD 28].

8.3 Intercomparison of MTCI and OTCI

Indirect verification of OTCI is conducted to examine its consistency to MTCI. This section presents an assessment of OTCI (2016-2020) as compared to the MERIS archive (2002-2012). The assessment includes OTCI data up to orbital cycle 52 which concluded on 05 April 2020. To perform the comparison, three by three pixel extractions were collected over 37 ESA Core and CEOS LPV validation sites (Table 18). The sites meet several criteria that make them suitable for validation activities: i) they include a range of representative land cover types, ii) spatially extensive and homogeneous, iii) relatively flat topography, iv) legacy of scientific activity. The temporal pixel profiles are quality controlled and comparison statistics are computed (Table 19) such as R^2, Normalised Root Mean Square Difference (NRMSD) and mean difference or Bias. The intercomparison exercise includes only sites that have 12 full months of data for both, MERIS and S3 OLCI. Climatology time-series and scatterplots of monthly OTCI mean are presented along with the statistical metrics.

The results show that for most of the sites there is good agreement between MTCI and OTCI (R^2>8.0), accuracy (NRMSD<0.1) and low absolute bias <0.2 (Table 19). There are sites such as AU-Calperun, NE-Loboos and US-Moab-Site that present lower R^2 ($\leqslant$60). These sites are characterised by subtle seasonality and interannual variations. However, in these sites, NRMSD remains low <0.05 (i.e. high accuracy). Overall, S3B presents similar results in terms of R^2 and NRMSD, however, a larger number of sites appear to have low R^2. S3B began operations on 23 November 2018; therefore it may still be early to draw robust conclusions on the intercomparison. Apart from those sites, S3B shows mean R^2>0.70 and mean NRMSD=0.07. Figure 23 illustrates the agreement of the products for three representative sites: FR-Montiers (DBF), IT-Lison (Cultivated) and BR-Mata-Seca (Non-forest). The sites in the northern hemisphere (FR-Montiers and IT-Lison) depict the beginning of the growing season, whereas the site in southern hemisphere (BR-Mata-Seca) is moving towards the end of the growing season. It is also evident that OTCI acquisitions for cycle 56 are in accordance with the seasonal trend and within ±SD of the climatology. Finally, when all sites are pooled together (Figure 24), agreement between MERIS and OLCI is high (R^2~9), NRMSD <0.1 for OTCI. A marginal negative bias is observed for OTCI (-0.015).

Table 18: Validation sites analysed in report S3A 56/S3B 37. Land cover data from GLC2000: shrub and herbaceous (Non-forest), broad-leaved evergreen (EBF), broad-leaved deciduous (DBF), evergreen needle-leaved (ENF), cropland, cultivated and managed areas (Cultivated).

No	Acronym	Network	Lat	Lon	Land cover
1	AU-Calperum	TERN-SuperSites, AusCover/OzFlux	-34.003	140.588	Non-forest
2	AU-Cape-Tribulation	TERN-SuperSites, OzFlux	-16.106	145.378	EBF
3	AU-Cumberland	TERN-SuperSites, AusCover/OzFlux	-33.615	150.723	EBF
4	AU-Great-Western	TERN-SuperSites, AusCover/OzFlux	-30.192	120.654	DBF
5	AU-Litchfield	TERN-SuperSites, AusCover/OzFlux	-13.180	130.790	EBF
6	AU-Robson-Creek	TERN-SuperSites, AusCover/OzFlux	-17.117	145.630	EBF
7	AU-Rushworth	TERN-AusCover	-36.753	144.966	DBF
8	AU-Tumbarumba	TERN-SuperSites, AusCover/OzFlux	-35.657	148.152	EBF
9	AU-Warra-Tall	TERN-SuperSites, AusCover/OzFlux	-43.095	146.654	EBF
10	AU-Watts-Creek	TERN-AusCover	-37.689	145.685	EBF
11	AU-Wombat	TERN-SuperSites, AusCover/OzFlux	-37.422	144.094	EBF
12	BR-Mata-Seca	ENVIRONET	-14.880	-43.973	Non-forest
13	CR-Santa-Rosa	ENVIRONET	10.842	-85.616	EBF
14	DE-Geb	CORE	51.100	10.914	Cultivated
15	DE-Selhausen	ICOS	50.866	6.447	Cultivated
16	FR-Aurade	ICOS	43.550	1.106	Cultivated
17	FR-Estrees-Mons	ICOS Associated	49.872	3.021	Cultivated
18	FR-Guayaflux	ICOS Associated	5.279	-52.925	EBF
19	FR-Montiers	ICOS	48.538	5.312	DBF
20	FR-Puechabon	ICOS	43.741	3.596	ENF
21	IT-Cat	CORE	37.279	14.883	Cultivated
22	IT-Collelongo	EFDC	41.849	13.588	DBF
23	IT-Lison	ICOS	45.740	12.750	Cultivated
24	IT-Tra	CORE	37.646	12.867	Cultivated
25	NE-Loobos	ICOS Associated	52.166	5.744	ENF
26	SE-Dahra	KIT / UC	15.400	-15.430	Cultivated
27	SP-Ali	CORE	38.452	-1.065	Cultivated
28	UK-NFo	CORE	50.845	-1.540	DBF
29	UK-Wytham-Woods	ForestGeo - NPL	51.774	-1.338	DBF
30	US-Bartlett	NEON, AERONET	44.064	-71.287	DBF
31	US-Central-Plains	NEON, AERONET	40.816	-104.746	Non-forest
32	US-Harvard	NEON, AERONET	42.537	-72.173	DBF
33	US-Moab-Site	NEON, AERONET	38.248	-109.388	Non-forest
34	US-Mountain-Lake	NEON, AERONET	37.378	-80.525	DBF
35	US-Oak-Rige	NEON, AERONET	35.964	-84.283	DBF
36	US-Talladega	NEON, AERONET	32.950	-87.393	ENF

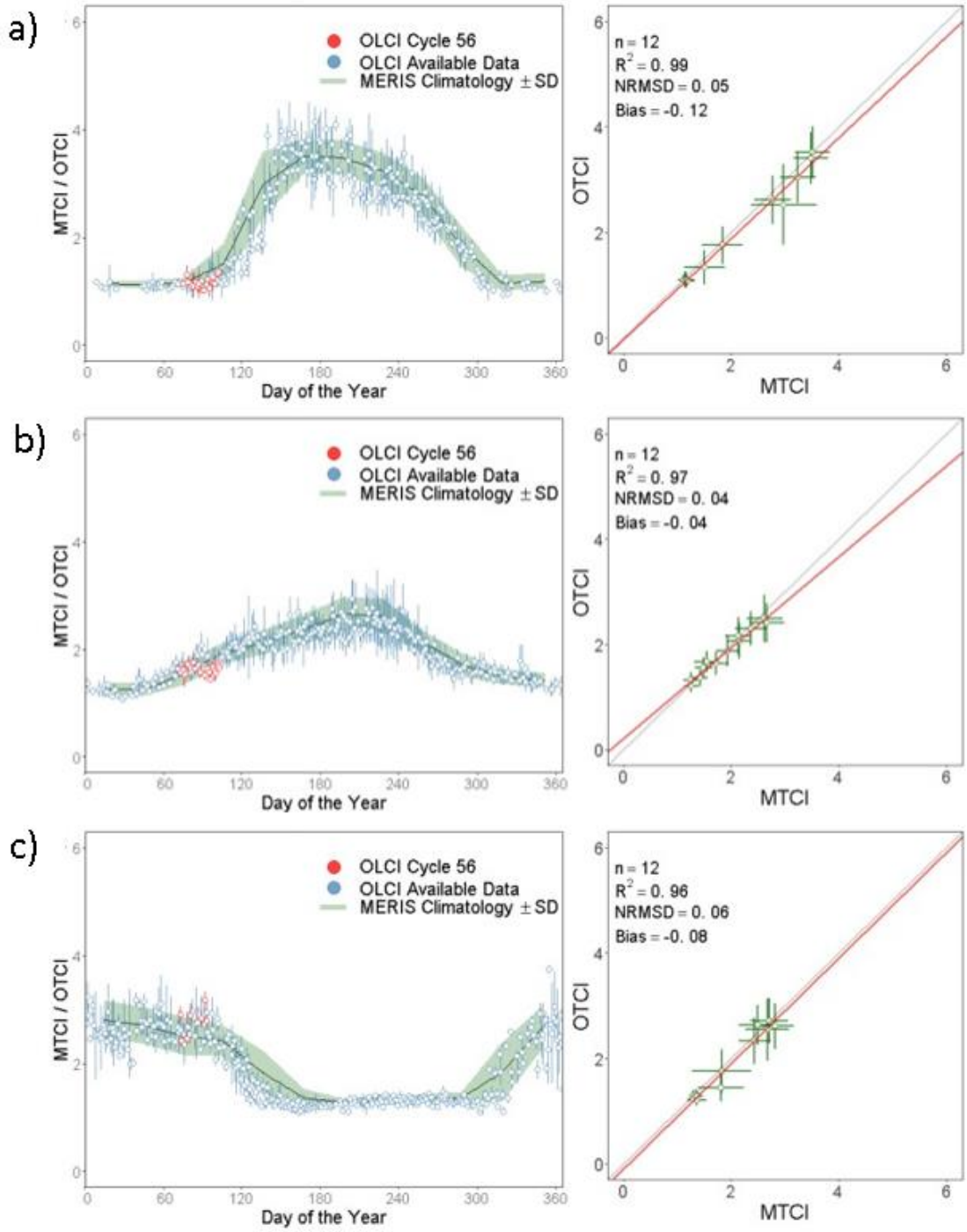

Figure 23: Time-series OTCI and corresponding scatterplot of monthly mean for sites: a) FR-Montiers, b) IT-Lison and c) BR_Mata Seca. On the time-series plots, in red appear the acquisitions within the time of the orbital cycle 56 (09 March 2020 and 05 April 2020). On the scatterplots, the grey line represents the 1:1 line whereas the red line is the linear model.

Table 19: Comparison statistics between monthly S3A/B OLCI land product OTCI and MTCI archive data.

No	Site Acronym	S3A				S3B			
		OTCI vs MTCI				OTCI vs MTCI			
		n	R2	NRMSD	Bias	n	R2	NRMSD	Bias
1	AU-Calperum	12	0.48	0.04	0.10	12	0.04	0.05	0.04
2	AU-Cape-Tribulation	12	0.81	0.05	-0.09	11	0.76	0.04	-0.20
3	AU-Cumberland	12	0.93	0.02	0.02	12	0.52	0.06	0.02
4	AU-Great-Western	12	0.96	0.02	0.13	12	0.90	0.02	0.14
5	AU-Litchfield	12	0.91	0.02	-0.01	12	0.62	0.08	0.01
6	AU-Robson-Creek	12	0.92	0.03	-0.06	11	0.79	0.05	-0.17
7	AU-Rushworth	12	0.84	0.04	0.20	12	0.17	0.09	-0.11
8	AU-Tumbarumba	12	0.81	0.06	0.36	12	0.62	0.08	0.19
9	AU-Warra-Tall	12	0.68	0.06	-0.03	7	0.52	0.08	-0.31
10	AU-Watts-Creek	12	0.70	0.05	0.10	12	0.65	0.06	0.04
11	AU-Wombat	12	0.89	0.04	0.19	12	0.63	0.05	-0.09
12	BR-Mata-Seca	12	0.96	0.06	-0.08	12	0.97	0.05	-0.10
13	CR-Santa-Rosa	12	0.98	0.04	0.13	12	0.84	0.12	-0.04
14	DE-Geb	12	0.86	0.11	-0.09	10	0.76	0.11	-0.04
15	DE-Selhausen	12	0.90	0.07	-0.02	11	0.68	0.10	-0.15
16	FR-Aurade	12	0.76	0.12	0.08	11	0.81	0.11	0.03
17	FR-Estrees-Mons	12	0.94	0.08	0.03	12	0.89	0.11	0.14
18	FR-Guayaflux	12	0.68	0.04	-0.16	11	0.81	0.03	-0.26
19	FR-Montiers	12	0.99	0.05	-0.12	11	0.98	0.06	-0.11
20	FR-Puechabon	12	0.69	0.05	-0.09	12	0.87	0.05	0.03
21	IT-Cat	12	0.63	0.04	-0.35	12	0.49	0.06	-0.31
22	IT-Collelongo	12	0.97	0.07	-0.02	11	0.80	0.23	0.01
23	IT-Lison	12	0.97	0.04	-0.04	11	0.90	0.06	-0.07
24	IT-Tra	12	0.79	0.02	-0.05	12	0.47	0.05	0.07
25	NE-Loobos	12	0.59	0.09	0.04	11	0.57	0.07	0.05
26	SE-Dahra	12	0.60	0.07	-0.03	8	0.04	0.16	-0.08
27	SP-Ali	12	0.92	0.02	0.07	12	0.88	0.03	0.11
28	UK-NFo	12	0.98	0.04	-0.25	10	0.97	0.04	-0.25
29	UK-Wytham-Woods	12	0.96	0.06	0.07	10	0.89	0.09	-0.17
30	US-Bartlett	12	0.95	0.05	0.03	11	0.84	0.09	-0.05
31	US-Central-Plains	12	0.73	0.03	-0.06	8	0.46	0.06	-0.09
32	US-Harvard	12	0.99	0.02	-0.14	11	0.98	0.05	-0.21
33	US-Moab-Site	12	0.60	0.02	0.05	11	0.53	0.04	0.01
34	US-Mountain-Lake	12	0.99	0.03	-0.22	11	0.97	0.05	-0.52
35	US-Oak-Rige	12	0.99	0.04	-0.06	12	0.98	0.06	-0.10
36	US-Talladega	12	0.97	0.02	-0.14	12	0.91	0.05	-0.18

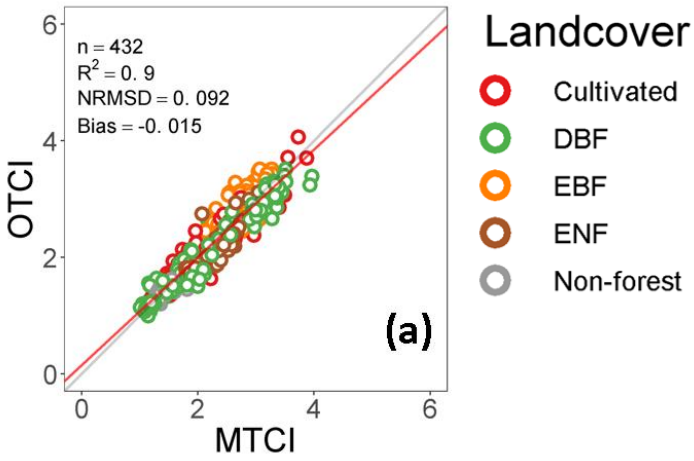

Figure 24: Comparison of MTCI vs OTCI. Points in the scatterplot represent the monthly mean of all available S3A and MERIS archive over 36 validation sites. Red and grey lines represent the modelled and 1:1 lines respectively. The scatterplots are updated to include extractions from cycle S3A 56. Land cover: Cultivated (managed areas and cropland), DBF (broadleaved deciduous), EBF (broadleaved evergreen), ENF (needleleaved evergreen), Non-forest (shrub and herbaceous).

9 MTCI Applications

The operational availability of the land product and the simplicity and efficiency of the MTCI algorithm facilitates multiple terrestrial applications as a satellite product and as a vegetation index. This section presents a few recent selected applications and a brief description of the study (Table 20).

Table 20: Examples of selected MTCI applications.

Application	Reference	Description
Phenology	He et al., (2015) [RD 31]	Phenological metrics estimated from both MERIS MTCI and GIMMS NDVIg were compared over China. The authors observed later end of season dates for MTCI.
	Tüshaus et al., (2014) [RD 32]	MTCI along with MODIS NDVI were used to investigate trends in irrigated croplands in Central Asia. The results confirmed an overall declining trend.
	Atkinson et al., (2012) [RD 33]	Four time-series smoothing techniques widely used land surface phenology studies were compared on MTCI and phenological metrics estimated over India.
GPP	Wang et al., (2019) [RD 34]	The maximum rate of carboxylation (Vcmax), was derived from MTCI and used to model GPP in evergreen needle-leaf forest in Canada. The incorporation of seasonal variations in Vcmax improved the model results when compared to flux tower measurements.
	Rossini et al., (2012) [RD 35]	NDVI, PRI and MTCI were computed from near-surface field spectroscopy and were employed to estimate GPP using a light use efficiency model in a subalpine grassland. The results indicated good correlation

		between modelled GPP and eddy covariance.
	Wu et al., (2009) [RD 36]	Several chlorophyll related vegetation indices calculated from canopy reflectance data were used in a GPP model that employs canopy chlorophyll content and PAR. When compared to ground truth data, the model that ingested MTCI had showed higher correlation to GPP.
Crop yield	Egea-Cobrero et al., (2018) [RD 37]	Integrated MTCI over the growing season was used to estimate crop yield in Andalusia region, Spain. The authors found statistically significant correlation between production, yield and MTCI at agricultural district level.
	Zhang et al., (2014) [RD 38]	NDVI and MTCI derived from MERIS surface reflectance were used to estimate crop yield in the Henan Province, China. The results indicated that correlation between yield and cumulative vegetation index was higher for MTCI than for NDVI.
Land cover mapping	Reese et al., (2007) [RD 39]	MERIS bands and MTCI were used to map Sweden mountain vegetation. The results indicated that including MTCI as a data layer in the classification improved the separation of land cover classes.
	Lyalko et al., (2006) [RD 40]	The land cover of the Ukranian Carpathians were classified using MERIS reflectance bands and MTCI. Given that MTCI is sensitive to a wide range of chlorophyll and relatively insensitive to topography, MTCI yielded better results than using the reflectance alone.
Health	Khwarahm et al., (2017) [RD 41]	Phenophases of birch and grass were mapped at country level in the UK to aid

		pollen forecast. This shows the potential of MTCI to provide more accurate spatially explicit information to pollen allergy sufferers.
Crop Chlorophyll	Peng et al., (2017) [RD 42]	Hyperspectral canopy reflectance, resampled to Sentinel-2 MSI spectral bands were used to derive 11 chlorophyll related vegetation indices. The study suggests that MTCI was less affected by crop hysteresis; this is, the index was linearly related to canopy chlorophyll content regardless of crop growing stage.
Canopy N	Loozen et al., (2018) [RD 43]	The relationship between N concentration and canopy N content and MTCI was investigated at regional scale in a Mediterranean forest. MTCI performed well in predicting both with some differences between plant functional types.
	Tian et al., (2011) [RD 44]	Two band and three band published and newly developed vegetation indices derived from hyperspectral canopy reflectance were compared to rice leaf N concentration. MTCI had similar performance to the newly developed indices.

10 Applicable Documents

[AD 1] Final Report “Validation of the ENVISAT MTCI geophysical product” ESTEC Contract No. 19957/NL/EL, 2006.

[AD 2] Chlorophyll Index ATBD Version – 2.2, Issue 1, Revision 2.

[AD 3] GMES Sentinel-3 Mission Requirements Document. EOP-SMO/1151/MDmd

[AD 4] QA4EO A Guide to expression of uncertainty of measurements. QA4EO-QAEO-GEN-DQK-006.

11 Reference Documents

[RD 1] Datt, B. (1998) 'Remote Sensing of Chlorophyll a, Chlorophyll b, Chlorophyll a+b, and Total Carotenoid Content in Eucalyptus Leaves', *Remote Sensing of Environment,* 66(2), 111-121

[RD 2] Gitelson, A., Merzylak, M.N. (1998) Remote sensing of chlorophyll concentration in higher plant leaves. *Advances in Space Research*, 22: 689-692

[RD 3] Mariotti, M., Ercoli, L. and Masoni, A. (1996) 'Spectral properties of iron-deficient corn and sunflower leaves', *Remote Sensing of Environment,* 58(3), 282-288

[RD 4] Daughtry, C.S.T, Walthall, C.L., Kim, M.S., Brown de Coulston, E., Mc Murtrey III, J.E. (2000) Estimating corn leaf chlorophyll concentration from leaf and canopy reflectance, *Remote Sensing of Environment*, 74: 229-239.

[RD 5] O'Neill, A. L., Kupiec, J. A. and Curran, P. J. (2002) 'Biochemical and reflectance variation throughout a Sitka spruce canopy', *Remote Sensing of Environment,* 80(1), 134-142

[RD 6] Peterson, D. L., Aber, J. D., Matson, P. A., Card, D. H., Swanberg, N., Wessman, C. and Spanner, M. (1988) 'Remote sensing of forest canopy and leaf biochemical contents', *Remote Sensing of Environment,* 24(1), 85-108

[RD 7] Coops, N. C., Stone, C., Culvenor, D. S., Chisholm, L. A. and Merton, R. N. (2003) 'Chlorophyll content in eucalypt vegetation at the leaf and canopy scales as derived from high resolution spectral data', *Tree Physiology,* 23(1), 23-31

[RD 8] Dash, J. and Curran, P.J. (2004) The MERIS terrestrial chlorophyll index. *International Journal of Remote Sensing*, 25: 5403-5413.

[RD 9] Richter, K., Rischbeck, P., Eitzinger, J., Schnieder, W., Suppan, F., Weihs, P. (2008) Plant growth monitoring and potential drought risk assessment by means of Earth Observation data. *International Journal of Remote Sensing*, Vol. 29 (17-18), p. 4943-4960.

[RD 10] ESA (2011) 'Sentinel-3' *ESA's Sentinel* Satellites European Space Agency (ESA) available at: http://www.esa.int/esaLP/SEMTST4KXMF_LPgmes_0.html, Last accessed; 17/03/2011.

[RD 11] Munden, R., Curran, P. J. and Catt, J. A. (1994) 'The relationship between red edge and chlorophyll concentration in the Broadwalk winter heat experiment at Rothamsted', *International Journal of Remote Sensing,* 15, 705-709

[RD 12] Lichtenthaler, H. K., Gitelson, A. and Lang, M. (1996) 'Non-Destructive Determination of Chlorophyll Content of Leaves of a Green and an Aurea Mutant of Tobacco by Reflectance Measurements', *Journal of Plant Physiology,* 148(3–4), 483-493

[RD 13] Baret, F., Foutry, T. (1997) Radiometric estimates of nitrogen status in crops, in Lemaire, G. (Ed), *Diagnosis of the Nitrogen Status in Crops*, New York, Springer-Verlag, p201-227.

[RD 14] Curran, P. J. (1989) 'Remote sensing of foliar chemistry', *Remote Sensing of Environment,* 30, 271-278

[RD 15] Curran, P. J. (1980) Multispectral remote sensing of vegetation amount. Prog. Phys. Geogr. Earth Environ. 4, 315–341.

[RD 16] Horler, D.N.H., Dockray, M., Barber, J. (1983) The red edge of plant leaf reflectance. *International Journal of Remote Sensing*, 4:273-288.

[RD 17] Curran, P. J., Dungan, J. L. and Gholz, H. L. (1990) 'Exploring the relationship between reflectance red edge and chlorophyll content in slash pine', *Tree Physiology,* 7, 33-48

[RD 18] Demetriades-Shah, T.H., Steven, M.D., Clark, J.A. (1990) High resolution derivative spectra in remote sensing. *Remote Sensing of Environment*, 33; 55-64.

[RD 19] Bonham-Carter, G.F. (1988) Numerical procedures and computer program for fitting an inverted Gaussian model to vegetation reflectance data. *Computers and Geosciences,* 14; 339-356.

[RD 20] Miller, J. R., Wu, J., Boyer, M. G., Belanger, M. and Hare, E. W. (1991) 'Seasonal pattern in leaf reflectance red-edge characteristic', *International Journal of Remote Sensing,* 12, 1509-1523

[RD 21] Guyot, G., Baret, F. and Major, D. (1988) 'High spectral resolution: Determination of spectral shifts between the red and the near infrared', *International Archives of Photogrammetry and Remote Sensing,* 11, 740-760

[RD 22] Danson, F.M., Plummer, S.E., (1995) Red edge response to forest leaf area index. *International Journal of Remote Sensing*, 16; 183-188.

[RD 23] Dawson, T. P. and Curran, P. J. (1998) 'A new technique for interpolating the reflectance red edge position', *International Journal of Remote Sensing,* 19, 2133-2139

[RD 24] Miura, T., Huete, A.R., Yoshioka, H. (2000) Evaluation of sensor calibration uncertainties on vegetation indices for MODIS. *IEEE Transactions on Geoscience and Remote Sensing*. Vol. 38, No. 3.

[RD 25] Verhoef, W., Bach, H. (2003) Simulation of hyperspectral and directional radiance images using coupled biophysical and atmospheric radiative transfer models. *Remote Sensing of Environment*. 87; 23-41

[RD 26] Schlapfer, D., Odermatt, D. (2006) *MODO User Manual*, version 3, ReSe Applications Schlapfer, Wil, Switzerland. Available at: http://www.rese.ch/pdf/MODO_Manual.pdf

[RD 27] Richter, K., Paladino, M., Vuolo, F., Dini, L., D'Urso, G. (2009) Spatial distribution of soil water content from airborne thermal and optical remote sensing data. In: SPIE's 2009

conference proceedings: Remote Sensing for Agriculture, Ecosyste,s and Hydrology XI, Vol. 7472, pp.74720W-74720W-11.

[RD 28] Brown, L.A.; Dash, J.; Lidón, A.L.; Lopez-Baeza, E.; Dransfeld, S. (2019) Synergetic exploitation of the Sentinel-2 missions for validating the Sentinel-3 ocean and land color instrument terrestrial chlorophyll index over a vineyard dominated mediterranean environment. IEEE J. Sel. Top. Appl. Earth Obs. Remote Sens. 12; 2244–2251.

[RD 29] Dash, J., Curran, P.J., Tallis, M.J., Llewellyn, G.M., Taylor, G., Snoeijf, P., 2010. Validating the MERIS terrestrial chlorophyll index (MTCI) with ground chlorophyll content data at MERIS spatial resolution. Int. J. Remote Sens. 31, 5513–5532. https://doi.org/10.1080/01431160903376340

[RD 30] Vuolo, F., Dash, J., Curran, P.J., Lajas, D., Kwiatkowska, E., 2012. Methodologies and Uncertainties in the Use of the Terrestrial Chlorophyll Index for the Sentinel-3 Mission. Remote Sens. 4, 1112–1133. https://doi.org/10.3390/rs4051112

[RD 31] He, Y., Bo, Y., de Jong, R., Li, A., Zhu, Y., & Cheng, J. (2015). Comparison of vegetation phenological metrics extracted from GIMMS NDVIg and MERIS MTCI data sets over China. *International Journal of Remote Sensing*, *36*(1), 300–317. https://doi.org/10.1080/01431161.2014.994719

[RD 32] Tüshaus, J., Dubovyk, O., Khamzina, A., & Menz, G. (2014). Comparison of medium spatial resolution ENVISAT-MERIS and terra-MODIS time series for vegetation decline analysis: A case study in central Asia. *Remote Sensing*, *6*(6), 5238–5256. https://doi.org/10.3390/rs6065238

[RD 33] Atkinson, P. M., Jeganathan, C., Dash, J., & Atzberger, C. (2012). Inter-comparison of four models for smoothing satellite sensor time-series data to estimate vegetation phenology. *Remote Sensing of Environment*, *123*, 400–417. https://doi.org/10.1016/j.rse.2012.04.001

[RD 34] Wang, R., Chen, J. M., Luo, X., Black, A., & Arain, A. (2019). Seasonality of leaf area index and photosynthetic capacity for better estimation of carbon and water fluxes in evergreen conifer forests. *Agricultural and Forest Meteorology*, *279*, 107708. https://doi.org/10.1016/j.agrformet.2019.107708

[RD 35] Rossini, M., Cogliati, S., Meroni, M., Migliavacca, M., Galvagno, M., Busetto, L., … Colombo, R. (2012). Remote sensing-based estimation of gross primary production in a subalpine grassland. *Biogeosciences*, *9*, 2565–2584. https://doi.org/10.5194/bg-9-2565-2012

[RD 36] Wu, C., Niu, Z., Tang, Q., Huang, W., Rivard, B., & Feng, J. (2009). Remote estimation of gross primary production in wheat using chlorophyll-related vegetation indices. *Agricultural and Forest Meteorology*, *149*(6–7), 1015–1021. https://doi.org/10.1016/j.agrformet.2008.12.007

[RD 37] Egea-Cobrero, V., Rodríguez-Galiano, V., Sánchez-Rodríguez, E., & García-Pérez, M. A. (2018). Wheat yield prediction in Andalucía using MERIS Terrestrial Chlorophyll Index (MTCI) time series. *Revista de Teledeteccion*, *2018*(51), 99–112. https://doi.org/10.4995/raet.2018.8891

[RD 38] Zhang, S., & Liu, L. (2014). The potential of the MERIS Terrestrial Chlorophyll Index for crop yield prediction. *Remote Sensing Letters*, *5*(8), 733–742. https://doi.org/10.1080/2150704X.2014.963734

[RD 39] Reese, H., Nilsson, M., & Olsson, H. (2007). Using MERIS for mountain vegetation mapping and monitoring in Sweden. In *European Space Agency (Special Publication), Proceedings of the ENVISAT Symposium* (pp. 23–27). Montreux, Switzerland.

[RD 40] Lyalko, V. I., Shportyuk, Z. M., Sakhatskyi, O. L., & Sybirtseva, O. M. (2006). Land cover classification in Ukrainian Carpathians using the MERIS Terrestrial Chlorophyl Index and red edge position from ENVISAT MERIS data. *Kosmichna Nauka i Tekhnologiya*, *12*, 10–14. Retrieved from https://ui.adsabs.harvard.edu/abs/2006KosNT..12f..10L

[RD 41] Khwarahm, N. R., Dash, J., Skjøth, C. A., Newnham, R. M., Adams-Groom, B., Head, K., … Atkinson, P. M. (2017). Mapping the birch and grass pollen seasons in the UK using satellite sensor time-series. *Science of the Total Environment*, *578*, 586–600. https://doi.org/10.1016/j.scitotenv.2016.11.004

[RD 42] Peng, Y., Nguy-Robertson, A., Arkebauer, T., & Gitelson, A. (2017). Assessment of Canopy Chlorophyll Content Retrieval in Maize and Soybean: Implications of Hysteresis on the Development of Generic Algorithms. *Remote Sensing*, *9*(3), 226. https://doi.org/10.3390/rs9030226

[RD 43] Loozen, Y., Rebel, K. T., Karssenberg, D., Wassen, M. J., Sardans, J., Peñuelas, J., & De Jong, S. M. (2018). Remote sensing of canopy nitrogen at regional scale in Mediterranean forests using the spaceborne MERIS Terrestrial Chlorophyll Index. *Biogeosciences*, *15*(9), 2723–2742. https://doi.org/10.5194/bg-15-2723-2018

[RD 44] Tian, Y. C., Yao, X., Yang, J., Cao, W. X., Hannaway, D. B., & Zhu, Y. (2011). Assessing newly developed and published vegetation indices for estimating rice leaf nitrogen concentration with ground- and space-based hyperspectral reflectance. *Field Crops Research*, *120*(2), 299–310. https://doi.org/10.1016/j.fcr.2010.11.002